Ecological Informatics 48 (2018) 198–214

Contents lists available at ScienceDirect

Ecological Informatics

journal homepage: www.elsevier.com/locate/ecolinf

Development of a mechanistic eutrophication model for wetland management: Sensitivity analysis of the interplay among phytoplankton, macrophytes, and sediment nutrient release

Dong-Kyun Kim, Aisha Javed, Cindy Yang, George B. Arhonditsis*

Ecological Modelling Laboratory, Department of Physical & Environmental Sciences, University of Toronto, Toronto, Ontario M1C1A4, Canada

ARTICLE INFO

Keywords:
Cootes paradise
Eutrophication modelling
Macrophytes
Phytoplankton
Self-organizing maps
Sensitivity analysis

ABSTRACT

Wetlands are important ecosystems that play a key role in flood control, nutrient sink, shoreline stability, and biodiversity conservation. Considerable attention has been placed globally on the assessment and restoration of degraded wetlands. Of particular concern is the Cootes Paradise marsh, one of the most degraded Great Lakes wetlands in Southern Ontario, which has experienced a 90% decline in macrophyte coverage over the past 50 years. In this study, we present a wetland eutrophication model that explicitly accounts for the ecological interplay among phytoplankton, macrophytes, and nutrient release from the sediments. We first reviewed the pertinent literature to compile the most commonly used macrophyte mathematical formulations and plausible parameter ranges of their major ecophysiological processes, adaptive strategies, and ecosystem functional roles, such as resource (nutrient, light, and oxygen) limitation, refuge effects, and allelopathic interactions. We then used two sensitivity analysis methods: conventional multiple-linear regression and Self-Organizing Maps (*SOM*) to evaluate the ability of our mechanistic model to capture different facets of the wetland functioning, including a potential non-linear shift from a turbid phytoplankton-dominated to a clear macrophyte-dominated state. Our analysis showed that the residual variability of the linear models varied from 7% to 37%, when ecological parameters are considered in the sensitivity analysis, and thus *SOM* analysis is more suitable to elucidate complex non-linear patterns and identify model sensitivity. Parameters related to the characterization of sediment processes (sediment porosity and vertical diffusivity) appear to be influential in shaping model predictions for variables of management interest, such as ambient total phosphorus (*TP*) or chlorophyll *α* (*Chlα*) concentrations, and macrophyte abundance. Our study also showed that the ability of submerged macrophytes to exploit the available underwater light is critical in our efforts to predict the outcome of their competition with phytoplankton.

1. Introduction

Wetlands are biologically diverse ecosystems with a number of important roles in the environment, such as carbon and nutrient sinks, flood control, shoreline stability, and water pollution mitigation. Wetlands have been incorporated globally in remedial strategies to filter pollutants and toxicants that would otherwise enter the ecosystems of interest (Craft, 1997; Verhoeven et al., 2006). Degradation and loss of ecologically and economically important wetland ecosystems has been a topical issue in environmental sciences, especially in the Great Lakes region where roughly 60 to 80% of the coastal wetlands have been lost since the arrival of the European settlers in the 1800s (Environment Canada, 2006; Smith et al., 1991). Many of these wetlands have become imperiled due to a variety of natural and anthropogenic disturbances, such as cultural eutrophication, land use changes (e.g., urbanization), increased water levels, and bio-perturbation by the invasive common carp, *Cyprinus carpio* (Croft and Chow-Fraser, 2007; Lougheed et al., 1998). Consequently, cooperative programs, such as the Great Lakes Wetlands Conservation Action Plan (*GLWCAP*), have been developed in an effort to create, reclaim, rehabilitate, and protect wetland habitat in the Great Lakes basin (Environment Canada, 2006).

Recent restoration efforts of degraded wetlands have been influenced by the growing evidence of the existence of two alternative stable states: a clear macrophyte-dominated state and a turbid phytoplankton-dominated state, typically associated with low and high nutrient concentrations, respectively (Scheffer, 1990). Both states are characterized by a suite of feedback mechanisms that reinforce their establishment.

* Corresponding author.
E-mail address: georgea@utsc.utoronto.ca (G.B. Arhonditsis).

https://doi.org/10.1016/j.ecoinf.2018.09.010
Received 26 June 2018; Received in revised form 7 September 2018; Accepted 11 September 2018
Available online 13 September 2018

Namely, dense phytoplankton populations significantly reduce the illumination of the water column, thereby leading to the disappearance of submerged vegetation (Scheffer et al., 1997). Aquatic food web structure may then change profoundly, as invertebrates that are associated with vegetation disappear and subsequently the birds and fish that feed upon them disappear as well (Carpenter, 1981; Kéfi et al., 2015; Suding et al., 2004). Submerged vegetation provides an important refuge against predation for many animals (e.g., large zooplankton against fish predation), and hence its disappearance may be responsible for dramatic shifts in many predator–prey relationships. The build-up of legacy nutrients in the sediments can exert similar control on the status of a wetland. The absence of submerged macrophytes rooted in the sediments together with the feeding behaviour of pollution-tolerant, benthivorous fish can accentuate the release of these historical nutrient loads through sediment resuspension, which further exacerbate the degree of wetland impairment (Scheffer et al., 2001). These self-stabilization mechanisms presumably increase the resilience of undesirable conditions and have been linked with the so-called hysteresis patterns, whereby a degraded (turbid) state cannot be restored by an equal-sized reversal of the external factors that originally led to the system collapse (Schallenberg and Sorrell, 2009; Scheffer et al., 2001). The likelihood of hysteresis can cause large losses of ecological resources in wetlands and may require drastic and expensive management interventions to successfully induce a shift to a more desirable ecosystem state. Management actions aiming to trigger shifts of degraded turbid, algal-dominated marshes to clear water, macrophyte-dominated systems typically focus on (*i*) the reduction of nutrient levels to decrease algal biomass, (*ii*) introduction of piscivores or removal of planktivores to control phytoplankton through trophic cascades, and (*iii*) elimination of benthivorous fish to increase water clarity (Scheffer et al., 2001).

A characteristic example of a degraded wetland is the Cootes Paradise marsh, located at the western end of Lake Ontario, on the west side of Hamilton Harbour (Fig. 1). Nutrient enrichment resulting from exogenous point and non-point nutrient loads from wastewater treatment plants (*WWTP*), combined sewer overflows (*CSOs*) and agricultural/urban runoff have rendered this shallow ecosystem as one of the most severely impaired wetlands in the Great Lakes area (Kim et al., 2016; Thomasen and Chow-Fraser, 2012). The overarching idea of the local remedial actions has been that Cootes Paradise marsh is capable of switching into a clearer state, but the remedial efforts to reduce external nutrient loading have not yet reached the critical levels that will allow the system to recover to its former clear state (Chow-Fraser, 2005). In 1997, for example, abnormally low spring temperatures caused a delay of fish migration into the marsh, which in turn alleviated the predation pressure of planktivorous fish on zooplankton, thereby resulting in a zooplankton-mediated improvement in water clarity as well as a proliferation of submergent vegetation in previously unvegetated shallow locations (Lougheed et al., 2004). The mechanisms that led to this short-lived event offer a working hypothesis to delineate the optimal management actions in the area, even though bio-manipulation practices, such as the physical exclusion of large carp from the system, suggest that the implementation of a single “shock therapy” measure may not be sufficient to establish a resilient clear state (Lougheed et al., 2004; Scheffer et al., 2001). In this context, Kim et al. (2016) highlighted the critical facets of the ecosystem functioning that will shape its future trajectory, including the broader implications of water level fluctuations for the interplay among physical, chemical, and biological components of Cootes Paradise along with the establishment of aquatic vegetation with sufficient density (> 20 stems m^{-2}) that could improve water quality and clarity by modulating nutrient dilution, increasing sediment stability, and reducing the wind-mediated, sediment resuspension in the marsh (Lougheed et al., 2004).

In light of the significant knowledge gaps, we present a process-based wetland model that aims to enhance our understanding of the complex dynamics of wetland ecosystems in general, and in particular of Cootes Paradise. In the first part of our modelling study, we provide an overview of our efforts to characterize the physiological processes and associated kinetics of macrophytes. We then introduce the wetland eutrophication model (*WEM*) designed to capture the complex ecological interplay among phytoplankton, macrophytes, and nutrient release from the sediments. Notwithstanding the strength of process-based models in elucidating ecological patterns (Cuddington et al., 2013), the appropriate level of complexity remains a controversial topic. According to the principle of parsimony (also known as Occam's razor), models should be as simple as possible, but not simpler to the extent that important facets of ecosystem dynamics are omitted (Blumer et al., 1987; Paudel and Jawitz, 2012). On the other hand, opting for more complex models entails the risk of mischaracterizing multiple processes and thus getting predictions that stem from multiple erroneous assumptions that cancel each other out (“*right results for the wrong reasons*”). In this regard, a critical *WEM* property would be its ability to predict the likelihood of an abrupt, non-linear shift from the current turbid-phytoplankton dominated state to its former clear-macrophyte dominated state based on sound ecological foundation. Our modelling exercise attempts to shed light on this central question by

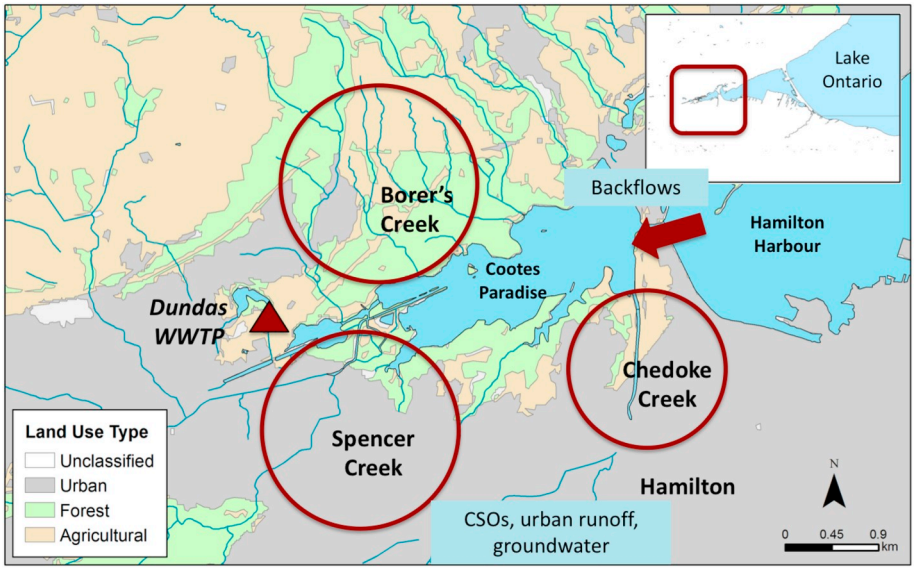

Fig. 1. Map identifying point and non-point sources in Cootes Paradise marsh. Point sources include the Dundas Waste Water Treatment Plant (*WWTP*) and Combined Sewer Overflows (*CSOs*). Non-point sources comprise tributaries, urban runoff, backflow from Hamilton Harbour, groundwater, and precipitation. The triangle indicates the Dundas *WWTP*, while the ellipsoids show the areas adjacent to the three major tributaries (Borer's Creek, Spencer Creek, and Chedoke Creek).

comparatively evaluating two methods of sensitivity analysis, linear regression and self-organizing map (*SOM*) analysis.

2. Materials and methods

2.1. Site description

Cootes Paradise marsh is a hyper-eutrophic shallow wetland that drains into the western end of Hamilton Harbour in Lake Ontario, Canada (Fig. 1). It contributes nearly 11% (40.8 kg day^{-1}) of the *TP* loading to the Hamilton Harbour and, according to recent modelling estimates, it is roughly responsible for 23% of the ambient *TP* variability in the system (Gudimov et al., 2010). It is approximately 4 km long, with a width of 1 km and a mean depth of 0.7 m. The hydraulic and nutrient loading of the marsh is predominantly driven by three main tributaries (Spencer, Chedoke and Borer's creeks) from the surrounding watershed, which contribute to its maximum surface area and volume of 2.50 km^2 and 3.57×10^6 m^3, respectively (Mayer et al., 2005). However, these dimensions vary considerably with water level fluctuations (Leisti et al., 2016). The marsh transitioned from a historically mesotrophic system to a eutrophic one in the 20th century when the surrounding forested areas were converted to agricultural and urban land uses. For the past nine decades, Cootes Paradise marsh has received nutrient inputs from agricultural run-off and multiple urban sources, such as effluent discharges from the Dundas *WWTP* and *CSO*s from the City of Hamilton (Routledge, 2012). Associated with the eutrophic trends in Cootes Paradise marsh has been the decline in vegetative cover from over 90% to < 15% along with a shift from its clear macrophyte-dominated to a turbid algal-dominated equilibrium state (Chow-Fraser, 2005). Until the late 1990s, the bio-perturbation by invasive common carp accelerated the degradation of aquatic vegetation in Cootes Paradise (Lougheed et al., 1998). In light of this degradation, a fishway barrier was constructed at the outlet of Cootes Paradise in 1997 in order to prevent large fish from entering the marsh and the average carp biomass per area for the entire marsh was reduced from 80 to 5 t km^{-2} (Lougheed et al., 2004; Theÿsmeÿer, 2011). Despite a great deal of restoration efforts, the improvement of water quality as well as the recovery of aquatic vegetation in the marsh remains an on-going challenge (Theÿsmeÿer et al., 2016).

2.2. Submerged macrophytes and mechanistic modelling

Macrophytes play a pivotal role in influencing the biogeochemical cycles and normal functioning of wetland ecosystems. Because of their importance in promoting the services provided by wetlands, recovery of submerged macrophytes has received considerable attention in aquatic ecosystem management. In this section, we first review some of the mathematical formulations proposed in the peer-reviewed literature to represent critical ecophysiological characteristics of submerged macrophytes (Tables 1–2). Since phosphorus has been historically considered as the primary factor to determine water quality in Cootes Paradise marsh, the current *WEM* version is founded upon a *P* mass-balance in the system. However, other nutrients, such as nitrogen and carbon, could also play a critical role in shaping macrophyte dynamics in the system. Nitrogen may directly or indirectly limit the primary production of macrophytes in fresh- and salt-water marshes (Tobias et al., 2001). To study the nitrogen cycling in a *Spartina alterniflora* saltwater marsh of Virginia (USA), Anderson et al. (1997) developed a process-based nitrogen mass-balance model by making use of measured microbial nitrogen cycling rates and estimates of above- and below-ground macrophytes, benthic microalgal production, as well as mass exchanges with the tidal creek, upland, and atmosphere. Sources and sinks of dissolved inorganic nitrogen (*DIN*) in the vegetated marsh were found to be balanced and maintained by temporarily immobilizing 50% of the mineralized *DIN* into a labile organic nitrogen pool, sequestered as ammonium. In addition to nitrogen, the three-dimensional hydrodynamical-biological model by Plus et al. (2003) considered the role of dissolved oxygen in Thau lagoon (situated in the Mediterranean coast of France). The impact of light on macrophyte photosynthesis was simulated using the hyperbolic tangential curve, while their gross production also considered nitrogen limitation based on the Wroblewski (1980) equation to take into account the preference of macrophytes for ammonium or nitrate (Short and McRoy, 1984). Macrophyte respiration and mortality were predominantly determined by the dissolved oxygen levels (Plus et al., 2003). Likewise, Park and Uchrin (1997) presented a model that simulated oxygen equivalents -founded upon a stoichiometric relationship between plant protoplasm and processes including photosynthesis, respiration, and death- nutrients and autochthonous organic matter.

In the context of light-limited growth, earlier work by Ikusima (1970) attempted to estimate the daily gross rate of photosynthesis in submerged and floating macrophytes according to a mathematical model that considered light attenuation with depth along with the structural profile of macrophyte communities. Considering the importance of minimum light on submerged macrophyte growth, Zimmerman et al. (1994) showed that daily integrated irradiance *I* is not a reliable predictor of daily production, and the same was true for analytical models based only on irradiance observations at noon. By contrast, the numerical integration of the daily period of *I*-saturated photosynthesis was much more reliable but required repeated *I* measures within a day. By recording winter time light attenuation spectra in a pristine mesotrophic lagoon, where phytoplankton concentrations and resuspension rates of sediments were fairly low, Domin et al. (2004) effectively modelled underwater light conditions and assessed the depth limits for the distribution of macrophytes. Herb and Stefan (2006) developed a simple, generic process-based macrophyte growth model to explicitly evaluate the effects of competition for light on growth of macrophyte species in temperate lakes. In comparison to monocultures, competitive growth was found to be more sensitive to basic physiological, morphological, and physical lake parameters. Invasive species were also shown to considerably suppress the growth of native species over a wide range of water depths and light conditions, primarily by reaching earlier the water surface and subsequently forming a dense surface canopy throughout the growing season (Herb and Stefan, 2006).

Regarding the control of invasive aquatic plants (e.g., *Myriophyllum spicatum L.*), Miller et al. (2011) modified the Herb and Stefan (2006) growth model by including additional variables that represented aggressive growth in the early season and the interaction with the watermilfoil weevil *Euhrychiopsis lecontei Dietz*. Alongside with the nutrient cycling and phytoplankton, there have been attempts to incorporate zooplankton and fish processes into the model structure to explore the refuge effect by macrophytes on zooplankton (Janse et al., 2010; Li et al., 2010; Lv et al., 2016; Xu et al., 1999; Zhang et al., 2003). Most of these recent modelling efforts of refuge effect of macrophytes are based on narrowly defined assumptions and are species-specific, and thus have limited potential for generalization (Lv et al., 2016). Similarly, the role of allelopathy has been reported to be unclear and a rather controversial means of phytoplankton control by macrophytes in the field, given that the isolation of the confounding effects of other processes controlling phytoplankton increase (e.g., shading, nutrient and light competition, increased water column stability) is often a difficult task. To overcome this problem, Mulderij et al. (2007) presented a phytoplankton growth model that incorporated the effects of shading, nutrient uptake, sediment resuspension, and excretion of allelopathic substances by two macrophytes (*Chara* sp. and *Stratiotes aloides*). The model showed that the relative contribution of allelopathy in situ was practically negligible for charophytes, whereas evidence of higher allelopathic potential was only provided for *S. aloides* (Mulderij et al., 2007).

In an attempt to connect macrophyte growth and decomposition with ecosystem processes in shallow eutrophic lakes, Asaeda et al.

Table 1
Characteristic examples of modelling studies that explicitly considered the role submerged macrophytes.

Phosphorus dynamics	
• A numerical model reproducing phytoplankton growth, macrophyte growth, macrophyte decomposition, and nutrient dynamics. Net macrophyte growth is modelled separately in five fractions (shoots, secondary shoots, roots, tubers and new tuber) as modulated by photosynthesis, respiration, mortality, and reallocation processes. Model provides information on total macrophyte biomass and phosphorus storage capacity.	Asaeda et al. (2001)
• The Kennet model characterizes phosphorus attached to suspended and river bed sediments, phosphorus uptake by epiphytes and macrophytes, and phosphorus exchange between water column and pore water.	Wade et al. (2001)
Nitrogen dynamics	
• Nitrogen mass-balance model incorporating gross mineralization, nitrification, denitrification, nitrogen fixation, above- and below-ground macrophyte production, and benthic microalgal production. The mass-balance model predicts annual balance between dissolved inorganic nitrogen sources (mineralization, nitrogen fixation, tidal creek fluxes, atmospheric deposition, and sediment inputs) and sinks (above- and below-ground macrophyte uptake, sediment microalgal uptake, sediment burial, microbial immobilization, denitrification, and nitrification).	Anderson et al. (1997)
• A three-dimensional model developed to examine the relationships between macrophytes and oxygen/nitrogen cycles. Model considers seven state variables (ammonia, nitrate, phytoplankton, zooplankton, detritus, oyster biodeposits, and oxygen), and six forcing factors (nitrogen inputs from watershed, light, water temperature, wind, oyster farming and macrophyte community). Nitrogen forms the basis of the model and dissolved oxygen is also incorporated to simulate processes, such as macrophyte photosynthesis (simulated using tangential hyperbolic P/I curve), macrophyte respiration (calculated as a function of temperature), and mineralization of organic matter.	Plus et al. (2003)
Light limitation	
• Approximation of light intensity at varying depths in submerged macrophyte communities using the Beer-Lambert's Law. Light condition assumed to be primarily influenced by plant shoot morphology, arrangement, and biomass. Light extinction coefficient of water is also considered to have an effect on the amount of light received by submerged macrophytes.	Ikusima (1970)
• One-compartment, simplified model of gross photosynthesis developed to provide an assessment of the amount of temporal irradiance data essential for accurate model predictions of the daily carbon gained by submerged macrophytes in coastal environments. Numerical (iterative) integration techniques and analytical (non-iterative) techniques are employed to estimate daily production.	Zimmerman et al. (1994)
• A general submerged macrophyte growth model incorporating physiological (growth rate, respiration rate, and biomass density) and physical (irradiance, water temperature, and water transparency) parameters. Growth rate is defined by the current biomass density (as opposed to being a function of time), while temperature and biomass are considered to be uniform over depth. Nutrient limitation is indirectly included in the model formulation through a growth rate coefficient.	Herb and Stefan (2003)
• Macrophyte light-dependent depth distribution is modelled based on chemical and physical properties and ecophysiological tolerance of macrophytes. Abiotic factors, such as salinity and currents, are assumed to be constant and the model overcomes missing historical light climate data by using recent measurements from reference conditions.	Domin et al. (2004)
• Macrophyte growth across varying light and temperature conditions are computed using the net daily production relationships established in Herb and Stefan (2003). The relationships from the original simple, generic growth model are broadened to evaluate the effect of light competition and non-uniform distribution of biomass on submerged macrophyte growth. Model formulation does not directly consider the influence of grazing and competition for nutrients among macrophyte species.	Herb and Stefan (2006)
Oxygen limitation	
• The SEMR1 (Shallow Impounded River Eutrophication Model, version 1), a one-dimensional model that considers the interactions related to water quality and aims to simulate the effects of macrophyte on dissolved oxygen, nutrient uptake/recycling, and release of organic matter. Aquatic plants (algae, periphyton, and macrophytes) are defined in terms of a time-dependent oxygen equivalent and first-order reactions characterize deoxygenation and sedimentation of carbonaceous biochemical oxygen demand.	Park and Uchrin (1997)
Allelopathy	
• Laboratory experiments conducted to determine the effect of macrophyte allelopathic activity on phytoplankton and filamentous algal densities. Nutrient (phosphate and potassium) limitation experiments were carried out to assess the change in sensitivity of phytoplankton cells to allelopathic substances under stress.	Mulderij et al. (2007)
Invasive plant control	
• A mathematical model that was used to evaluate the efficacy of native larva predation on controlling the population of invasive submerged plants. The invasive submerged plant model is a modified version of Herb and Stefan (2006)'s growth model, which considers water depth, water clarity, water temperature, and irradiance as the main factors influencing plant growth. Differences among developmental stages of the weevil are captured through an age-structured population model.	Miller et al. (2011)
Refuge effect	
• A mathematical model describing and simulating the refuge effect of submerged macrophytes. Nutrition, phytoplankton, submerged macrophytes, zooplankton, and fish are considered as key state variables. Model is developed based on the hypothesis that the refuge effect of submerged macrophytes results in a decreased rate of fish capture, encounter rate, swimming speed, visual field, foraging success and an increased handling time and attack ratio.	Li et al. (2010)
• A four-dimensional mechanistic model developed to evaluate the effect of changes in biomass density of submerged macrophytes in providing refuge to zooplankton and ultimately shape the interactions among phytoplankton, zooplankton, and fish. The predation relationship is formed using the Holling time budget arguments and phytoplankton and macrophyte are assumed to follow the conventional Lotka–Volterra competition model in the absence of zooplankton and fish.	Lv et al. (2016)
Interactions between multiple state variables	
• A numerical model integrating three submodels that evaluate the development of phytoplankton, sediment and nutrient dynamics, and growth of submerged macrophytes. Resuspension of sediments, effect of allelopathy on algal growth, decline in biomass as a result of wave action, and the impact of epiphyton were all omitted from the model in order to focus on basic ecological mechanisms.	Asaeda and Van Bon (1997)
• The Kennet model, a dynamic mathematical model operating on a daily time step, attempts to simulate phosphorus cycling among the water column, sediments, and biota (macrophytes and epiphytes). Biomass is used as a descriptor of macrophyte (combination of submerged and emergent species) and epiphyte growth. The rates of mass transfer between major phosphorus stores are modelled as first-order exchanges and portrayed as parameters in mass-balance equations.	Wade et al. (2002a, 2002b)
• Total phosphorus mass-balance model integrating macrophyte dynamics, directly assessing the role of dreissenids, and simulating the interplay between water column and sediments.	Gudimov et al. (2015), Kim et al. (2013)

Table 2
Literature review of physiological parameters for three types of macrophytes (emergent, submerged, and floating) in wetland ecosystems. Presence or absence of macrophyte species in Cootes Paradise (CP) is based on Lundholm and Simser (1999) and Thomasen and Chow-Fraser (2012).

Parameters	Presence in CP	N	Max	Min	Mean	SD	References
Growth rate, $\omega G_{(j)}$ (day^{-1})							
Emergent							
Phragmites australis	Yes	1	–	–	0.11*	–	Asaeda and Karunaratne (2000)
Submerged							
Ceratophyllum demersum	Yes	2	0.21	0.026	0.12	0.13	Herb and Stefan (2003)
Elodea canadensis	Yes	2	0.093	0.052	0.073	0.029	Herb and Stefan (2003)
Hydrilla verticillata	No	2	0.17	0.1	0.14	0.049	Herb and Stefan (2003)
Myriophyllum spicatum	Yes	3	0.18	0.09	0.13	0.046	Herb and Stefan (2003)
Potamogeton pectinatus	Yes	4	0.17	0.065	0.13	0.06	Herb and Stefan (2003)
Potamogeton praelongus	No	1	–	–	0.078	–	Herb and Stefan (2003)
Floating							
Eichhornia crassipes	No	1	–	–	0.012*	–	Pelton et al. (1998)
Lemna minor	Yes	1	–	–	0.07	–	Tabou et al. (2014)
Half-saturation constant, K_L (μg P L^{-1})							
Submerged							
Elodea canadensis	Yes	18	273	27.0	158	69.0	Christiansen et al. (2016)
Potamogeton pectinatus	Yes	1	–	–	5	–	Asaeda and Van Bon (1997)
Littorella uniflora	No	6	76.3	26.4	51.3	26.7	Christiansen et al. (2016)
Myriophyllum alterniflorum	No	3	–	–	126	51.2	Christiansen et al. (2016)
Floating							
Lemna minor	Yes	1	–	–	1260	–	Tabou et al. (2014)
Light-attenuation coefficient, $kext_{SUB}$ (m^2 g^{-1})							
Submerged							
Ceratophyllum demersum	Yes	1	–	–	0.016	–	Herb and Stefan (2003)
Elodea canadensis	Yes	1	–	–	0.018	–	Herb and Stefan (2003)
Hydrilla verticillata	No	1	–	–	0.01	–	Herb and Stefan (2003)
Myriophyllum spicatum	Yes	2	0.019	0.006	0.013	0.009	Herb and Stefan (2003)
Potamogeton pectinatus	Yes	1	–	–	0.02	–	
Potamogeton praelongus	Yes	1	–	–	0.01	–	Herb and Stefan (2003)
Mortality rate, $\omega_{D(j)}$ (day^{-1})							
Emergent							
Phragmites australis	Yes	2	0.0045	0.0005	0.003	0.003	Asaeda et al. (2001)
Submerged							
Myriophyllum heterophyllum	No	1	–	–	0.037	–	Asaeda et al. (2001)
Potamogeton pectinatus	Yes	2	0.082	0.0097	0.05	0.05	Asaeda et al. (2001)
P fraction of biomass, $\mu_{P/DW}$ (g P g dw^{-1})							
Emergent							
Bidens beckii	No	4	–	–	0.0032	0.0002	Carignan and Kalff (1982)
Iris pseudacorus	Yes	6	0.0153	0.0044	0.0088	0.0003	Li et al. (2015)
Oenanthe javanica	No	6	0.008	0.003	0.0057	0.0001	Li et al. (2015)
Phragmites australis	Yes	3	–	–	0.0003	0.00001	Li et al. (2013)
Typha angustifolia	Yes	3	–	–	0.0007	0.00004	Li et al. (2013)
Meadow							
Canna lily	No	6	0.012	0.004	0.0083	0.0001	Li et al. (2015)
Submerged							
Egeria densa	No	20	0.005	0.003	0.0041	0.0003	Barko and Smart (1980)
Elodea canadensis	Yes	6	–	–	0.0029	0.0003	Carignan and Kalff (1982)
Heteranthera dubia	No	4	–	–	0.0027	0.0003	Carignan and Kalff (1982)
Hydrilla verticillata	No	20	0.0067	0.0034	0.0052	0.0005	Barko and Smart (1980)
Myriophyllum alterniflorum	No	4	–	–	0.0038	0.0003	Carignan and Kalff (1982)
Myriophyllum spicatum	Yes	31	0.0061	0.0001	0.0031	0.0002	Barko and Smart (1980), Carignan and Kalff (1982)
Potamogeton crispus	Yes	4	0.0045	0.0032	0.0038	0.0001	Li et al. (2015)
Potamogeton foliosus	Yes	6	–	–	0.0026	0.0002	Carignan and Kalff (1982)
Potamogeton pectinatus	Yes	1	–	–	0.0013	0.0003	Li et al. (2013)
Potamogeton zosteriformis	No	4	–	–	0.0032	0.0002	Carignan and Kalff (1982)
Floating							
Ceratophyllum demersum	Yes	3	–	–	0.0034	0.00014	Li et al. (2013)
Lemina minor	Yes	3	–	–	0.0024	0.0002	Li et al. (2013)
Nelumbo nucifera	No	3	–	–	0.0017	0.00011	Li et al. (2013)
P uptake rate (mg P m^{-2} day^{-1})							
Emergent							
Carex virgata	No	1	–	–	0.5	–	Tanner and Headley (2011)
Iris spp.	Yes	2	40.3	9.3	24.8	21.9	Korboulewsky et al. (2012), Keizer-Vlek et al. (2014)
Phragmites australis	Yes	2	25.48	12.33	18.9	9.3	Kuusemets and Lohmus (2005), Korboulewsky et al. (2012)
Polygonum barbatum	No	1	–	–	0.4	–	Wang et al. (2015)
Schoenoplectus tabernaemontani	No	1	–	–	0.87	–	Tanner and Headley (2011)
Scirpus sylvaticus	No	1	–	–	39.7	–	Kuusemets and Lohmus (2005)

(*continued on next page*)

Table 2 (*continued*)

Parameters	Presence in CP	N	Max	Min	Mean	SD	References
Typha angustifolia	Yes	1	–	–	1.57	–	Wang et al. (2015)
Typha latifolia	Yes	1	–	–	16.99	–	Korboulewsky et al. (2012)
Meadow							
Chrysopogon zizanioides	No	1	–	–	0.2	–	Wang et al. (2015)
Cyperus ustulatus	No	1	–	–	8.5	–	Tanner and Headley (2011)
Juncus edgariae	No	1	–	–	5.2	–	Tanner and Headley (2011)
Submerged							
Egeria densa	No	2	2.88	1.64	2.26	0.87	Barko and Smart (1980)
Hydrilla verticillata	No	2	0.27	1.37	0.82	0.77	Barko and Smart (1980)
Myriophyllum spicatum	Yes	2	4.38	0.41	2.4	2.81	Barko and Smart (1980)
Mix of:		1	–	–	6.5	–	Julian et al. (2011)
▪ *Potamogeton crispus*	Yes						
▪ *Potamogeton pusilus*	Yes						
▪ *Potamogeton foliosis*	Yes						
▪ *Zosterella dubia,*	No						
▪ *Elodea canadensis*	Yes						
▪ *Nitella* spp.	No						
Respiration rate, $\omega R_{(j)}$ (day^{-1})							
Submerged							
Ceratophyllum demersum	Yes	1	–	–	0.009	–	Herb and Stefan (2003)
Elodea canadensis	Yes	2	0.023	0.018	0.021	0.004	Herb and Stefan (2003)
Hydrilla verticillata	No	1	–	–	0.018	–	Herb and Stefan (2003)
Myriophyllum spicatum	Yes	2	0.026	0.019	0.023	0.005	Herb and Stefan (2003)
Potamogeton pectinatus	Yes	2	0.005	0.013	0.012	0.007	Herb and Stefan (2003)
Potamogeton praelongus	Yes	1	–	–	0.022	–	Herb and Stefan (2003)

* Literature values converted to our model units by assuming that P fraction of macrophyte biomass is 15 g·P g·dw^{-1} for emergent and floating plants.

(2001) presented one of the few complex numerical models in the pertinent literature. A novel feature of the same study is that the growth of *Potamogeton pectinatus* L. was modelled by splitting biomass into five fractions: shoots, secondary shoots, roots, tubers and new tubers. Macrophytes were shown to increase with rising water temperatures and outcompete phytoplankton under favorable light conditions. In the same context, Wade et al. (2001) introduced a model that considered the exchange of *P* between water column and pore water, the interplay of *P* between suspended and bed sediments, and the uptake of *P* by epiphytes and macrophytes. In a subsequent study, the same model was applied to a reach of the River Kennet in south England to show that flow is more important in controlling macrophyte biomass than in-stream phosphorus concentrations (Wade et al., 2002b). Janse et al. (2010) used the PCLake model to shed light on the most important ecological interactions that establish the state (clear vs. turbid) of shallow lakes. The model considers a wide range of biotic variables (phytoplankton, submerged macrophytes, and a simplified food web comprising zooplankton, zoobenthos, young and adult whitefish, piscivorous fish), abiotic factors (e.g., nutrients), and the dynamics in the sediment top layer. Along the same line of thinking, a complex *TP* mass-balance model was employed to connect water quality conditions with exogenous *TP* loading and internal nutrient recycling, as modulated by the role of macrophyte and dreissenid mussels, in the Bay of Quinte and Lake Simcoe, both in Southern Ontario, Canada (Gudimov et al., 2015; Kim et al., 2013).

2.3. Characterization of submerged macrophyte processes and associated uncertainty

Empirical and modelling evidence suggests that growth rates for submerged macrophytes tend to be higher than those for meadow and emergent plants, although the sample sizes are not always statistically robust (Asaeda and Karunaratne, 2000; Herb and Stefan, 2003; Pelton et al., 1998; Tabou et al., 2014). Invasive species, such as the emergent *Phragmites*, dominate Cootes Paradise and are therefore regarded as a major threat to native vegetation (Theÿsmeÿer et al., 2016; Theÿsmeÿer and Bowman, 2017). Reported counts and actual values for the corresponding average growth rate (0.11 day^{-1}, $N = 1$) are much lower than those for the native submerged macrophyte species, such as *Ceratophyllum* (0.12 day^{-1}, $N = 2$), *Myriophyllum* (0.13 day^{-1}, $N = 3$), and *Potemogeton* (0.13 day^{-1}, $N = 4$) in Cootes Paradise (Table 2). Growth rates may significantly vary with the macrophyte composition, and thus models can potentially mischaracterize nutrient dynamics in wetlands depending on the succession patterns of aquatic vegetation.

Published information on the characterization of phosphorus uptake kinetics (e.g., half-saturation constant) is rather scarce and is restricted to a small number of macrophyte species. For example, half saturation constant values related to emergent and meadow macrophytes in wetland ecosystems are completely missing and even the values that are available, vary considerably among (5 μg *P* L^{-1} for *Potamogeton* spp. and 1260 μg *P* L^{-1} for the common duckweed, *Lemna minor*) and within individual species (e.g., 27–273 μg *P* L^{-1} for *Elodea*) (Table 2). Little experimental work has been carried out to determine these half saturation constants in situ, and instead ecological models are typically fit to field population data in order to indirectly calculate their values through inverse model solution exercises (Mulder and Hendriks, 2014). In a similar manner, the wide range of phosphorus uptake rates for meadow, emergent and submerged macrophytes from literature can significantly increase the predictive uncertainty (Table 2). Even within a particular functional macrophyte group, there is considerable variability in phosphorus uptake rates across species or genera (0.4–39.7 mg *P* m^{-2} day^{-1} for emergent, 0.2–8.5 mg *P* m^{-2} day^{-1} for meadow, and 0.82–6.5 mg P m^{-2} day^{-1} for submerged plants). In particular, among the macrophytes recorded in Cootes Paradise marsh, iris (*Iris* spp.) has the highest (24.8 mg *P* m^{-2} d^{-1}) and reed (*Phragmites australis*) the second highest (18.9 mg *P* m^{-2} d^{-1}) reported phosphorus uptake rates. In contrast, cattail (*Typha* spp.) and the Eurasian watermilfoil (*Myriophyllum spicatum*) are reported to having significantly lower mean phosphorus uptake rates, i.e., 1.57–17.0 mg *P* m^{-2} day^{-1} and 2.4 mg *P* m^{-2} day^{-1}, respectively (Table 2).

The phosphorus quota within macrophyte tissues ($\mu_{P/DW}$) is another important factor that can influence both phosphorus sequestration and recycling. For instance, a high $\mu_{P/DW}$ value can accelerate phosphorus cycling by increasing the amount of phosphorus uptake per unit of biomass produced, as well as its loss rates through basal metabolism. In reality though, phosphorus retention within the plant tissues can be

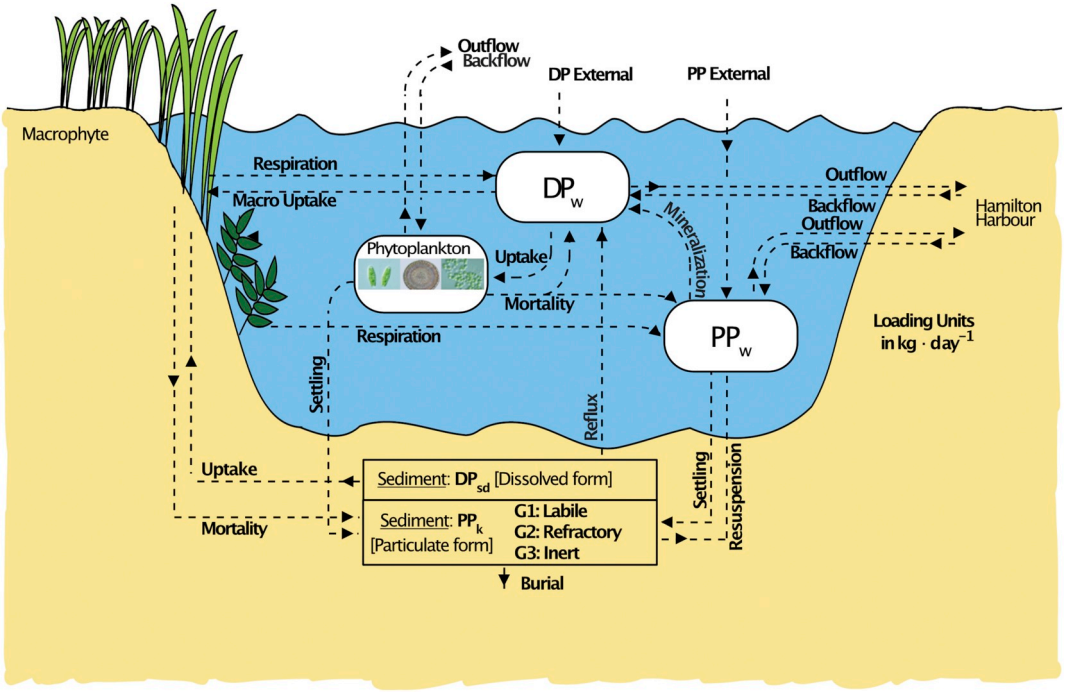

Fig. 2. Conceptual diagram of the Wetland Eutrophication Model (*WEM*) consisting of the following state variables: dissolved and particulate phase phosphorus in the water column, three functional phytoplankton and macrophyte (meadow, emergent and submerged) groups, sediment particulate phosphorus in labile, refractory, and inert forms, as well as dissolved phosphorus in interstitial waters.

more complicated, and is significantly shaped by different physiological strategies for nutrient storage and senescence. Phosphorus translocated to below-ground biomass (roots and rhizomes) generally represents a long-term storage pool, whereas the phosphorus pool in above-ground plant tissues (e.g., shoots) can be released into the water column within a shorter time-frame. On the other hand, phosphorus loss from decaying macrophytes due to leaching is independent of temperature and fragmentation of plant material, but does increase with higher allocation of phosphorus to more leachable *P* pools within the macrophytes (Carpenter, 1981). Bearing in mind the critical importance of $\mu_{P/DW}$ for establishing defensible *TP* budgets in wetland systems, Table 2 shows that there is considerable inter- and intra-specific variability. According to Granéli and Solander (1988), challenges associated with the specification of realistic values may arise from spatial and temporal variations, as well as the variability of macrophyte phosphorus content among different organs (e.g. leaves, culms, roots). *P* concentrations in living tissues are reported to vary between 0.0001 and 0.005 g *P* g dw^{-1} (Granéli and Solander, 1988). Likewise, significant variability exists in the reported respiration rates of submerged macrophytes, including Canadian Pondweed, *Elodea Canadensis* (0.018–0.023 day^{-1}); Eurasian water-milfoil, *Myriophyllum spicatum* (0.019–0.026 day^{-1}); and sago pondweed, *Potamogeton pectinatus* (0.005–0.013 day^{-1}) (Herb and Stefan, 2003). Similar to respiration, mortality rates also show significant variability (0.0005–0.0045 day^{-1} for emergent reed; 0.037 day^{-1} for submerged broadleaf watermilfoil, *Myriophyllum. heterophyllum*; and 0.0097–0.082 day^{-1} for submerged sago pondweed (Asaeda et al., 2001).

Few studies have also attempted to quantify self-shading and competitive light-shading effects between phytoplankton and submerged macrophytes. Invasive macrophyte species, such as the Eurasian watermilfoil, curly-leaf pondweed, *Potamogeton crispus*, and hydrilla, *Hydrilla verticillate*, influence the illumination of the water column by undergoing rapid growth in shoots towards the water surface and subsequent formation of dense surface canopies (Herb and Stefan, 2006). Additionally, broad-leaved submerged macrophytes in Cootes Paradise (e.g., curly-leaf pondweed and pondweed, *Potamogeton perfoliatus*) have the potential to shade the narrow-leaved macrophytes (e.g., small pondweed, *Potamogeton berchtoldii*, and sago pondweed). The variability in the light attenuation coefficient (0.01–0.02 $m^2\ g^{-1}$) for submerged species can therefore be attributed to variant morphological features that give rise to differential shading characteristics even within a single macrophyte genus, like the *Potamogeton* species (Table 2). As demonstrated in this section, a common recurring issue is the significant intra- and inter-specific variability for various important macrophyte parameter values. This variance may also stem from the lack of sufficient experimental work, and inconsistencies in the units employed by existing studies (and therefore the need for assumptions to convert them into identical units). Even with the increased granularity of our simulated macrophyte assemblage (i.e., multiple functional groups instead of a total macrophyte compartment), it must be emphasized that the parameters (e.g., rates, kinetics, nutrient quotas) used are "effective" and thus the values assigned after a model fitting exercise represent single estimates derived from fairly wide ranges of all the major ecophysiological macrophyte processes.

2.4. Model description

WEM is an augmentation of the simple *TP* mass-balance model developed by Kim et al. (2016), given that the limited empirical information about the role of nitrogen and practically no carbon data pose challenges to reasonably constrain the relevant submodels in Cootes Paradise. Our modelling exercise is based on a 17-year (1996–2012) study period and encompasses the same external forcing (meteorological and hydrological) data as the original model. While the previous simple mass-balance model dealt with both ambient and sediment *TP* as an aggregate variable, the current *WEM* version partitions the phosphorus pool into several distinct fractions and considers critical biogeochemical processes that shape the interplay among phytoplankton, macrophytes, and sediment nutrient release. Ambient *TP* pool has been divided into three fractions: (*i*) dissolved phosphorus (DP_w), (*ii*) particulate phosphorus (PP_w), and (*iii*) phosphorus sequestered in phytoplankton (Fig. 2). *TP* in the sediments has been separated into

dissolved phosphorus in the interstitial pore water (DP_{sd}), and three types of particulate phosphorus ($PP_{k=G1,G2,G3}$; labile, refractory, and inert) based on characterization presented in earlier modelling work (Cerco and Cole, 1994). Complete ordinary differential equations are presented in the Supporting Information (Table S1).

2.4.1. Phosphorus in water column

As previously mentioned, ambient *TP* is represented as the sum of dissolved (DP_w), particulate (PP_w), and phosphorus sequestered in phytoplankton. The relative amount of each of the three components in the water column *TP* is modulated by a suite of biogeochemical processes: uptake, mortality, mineralization, resuspension, decomposition, diffusion, settling, and respiration (Fig. 2). In contrast to the simple *TP* mass-balance model (Kim et al., 2016), the *WEM* governing equations consider macrophyte and phytoplankton DP_w uptake, while dead algal cells and macrophyte tissues replenish the PP_w pool. Exogenous PP_w inflows originate from *WWTP*, *CSO*s, urban runoff, groundwater, precipitation, and three major tributaries (i.e., Spencer, Chedoke and Borer's creeks). *WWTP* discharges are assumed to have an equal fraction of DP_w and PP_w, while DP_w from *CSO*s is calculated based on a DP_w:PP_w ratio of 0.19 derived by Wang (2014). To determine DP_w inputs from the three major tributaries, we used the annual average DP_w:*TP* ratios, as derived from measured values, and then multiplied them by the daily tributary loading. Mathematical details of the model processes are provided in Table S1. Phosphorus exchange between Cootes Paradise and Hamilton Harbour were kept the same as with the original *TP* mass-balance model.

2.4.2. Phosphorus in the sediments

The sediment submodel comprises dissolved phosphorus (DP_{sd}) in the interstitial pore water and particulate phosphorus (PP_k) (Fig. 2). PP_k continuously releases DP_{sd} through temperature-dependent decomposition. Based on empirical evidence from the system, sediment temperature is assumed to follow a sinusoidal seasonal pattern between 3 °C and 20 °C. DP_{sd} is lost through macrophyte uptake and sediment diffusive reflux, while PP_k is removed through sediment resuspension and burial. The rate of sediment resuspension into the water column is simulated by postulating a power-law relationship with bed shear stress (Chung et al., 2009; Kim et al., 2013; Mehta et al., 1982). The burial process to the deeper sediments (a closure term in our model) is determined by dividing the time-variant phosphorus mass in the sediments by a deposition coefficient. The latter coefficient determined the fraction of sediment phosphorus pool disappearing each day through the burial process, and was a function of the tributary sediment input divided by a "sediment factor". The sediment factor is in turn defined as a function of sediment thickness, porosity (i.e., sediment water content, %), and sediment solid density. Following the work of Minns (1986), the tributary sediment input was calculated by dividing a fixed suspended sediment concentration in the tributary inputs by the average annual tributary flow across the entire historical period (1996–2012). The inter-annual variability is then accommodated by multiplying the sediment input by the year-specific average daily tributary flow.

2.4.3. Phytoplankton

Following the local phosphorus-abatement efforts, through conversion of the Dundas *WWTP* to a tertiary-treatment facility, the phytoplankton community has experienced distinct structural shifts since the early 1990s (Chow-Fraser et al., 1998). In particular, the diversity of chlorophytes has increased and is now primarily dominated by species of the following genera: *Carteria, Chlamydomonas, Chlorella, Chlorococcus, Coccomonas, Gonium, Planktosphaeria,* and *Scenedesmus.* Chrysophytes (*Chromulina, Ochromonas*) have resurged into the marsh, reflecting a return to less eutrophic conditions. On the other hand, the continuous presence of cryptomonads (*Cryptomonas, Rhodomonas*) and euglenophytes (*Euglena, Lepocinclis, Phacus*) is likely associated with the poor illumination that still characterizes the water column. Diatoms (*Bacillariophyceae*) such as *Amphora, Gyrosigma, Melosira, Nitzschia,* and *Synedra* are typically present throughout the marsh, whereas cyanobacteria are no longer prominent in the algal community (Chow-Fraser et al., 1998). The *WEM* phytoplankton submodel is based on previous work by Arhonditsis and Brett (2005) and Ramin et al. (2011). We explicitly model three phytoplankton functional groups on the basis of their physiological characteristics. A diatom-like group represents an '*r*-strategist' with fast growth/metabolic rates, fast settling rates, and superior phosphorus kinetics, whereas a cyanobacteria-like group resembles to a '*K*-strategist' which is also characterized by slow settling rates, and inferior phosphorus kinetics. We also considered a third group specified as an intermediate between diatoms and cyanobacteria. Phytoplankton growth explicitly considers luxury uptake based on the assumption that phytoplankton nutrient uptake depends on both internal and external concentrations and is confined by a lower and upper bound (Asaeda and Van Bon, 1997; Arhonditsis and Brett, 2005; see also Table S1). Among a variety of established mathematical formulations pertinent to photosynthesis, we used Steele's equation with Beer's Law to scale diminishing light availability over depth. The extinction coefficient was calculated as the light attenuation stemming from phytoplankton and macrophyte abundance as well as the so-called inherent optical properties of water (or background attenuation). The optimal levels of light intensity and temperature for phytoplankton were based on modelling studies in Lake Ontario (Gudimov et al., 2010; Kim et al., 2013; Ramin et al., 2011). Basal metabolism of phytoplankton collectively accounts for all internal processes responsible for biomass decline, such as excretion, respiration, and natural mortality. Similar to previous modelling studies (Arhonditsis and Brett, 2005; Ramin et al., 2011), the basal metabolism is assumed to increase exponentially with temperature.

2.4.4. Macrophytes

As previously mentioned, the macrophyte community has experienced a significant decline in Cootes Paradise marsh over the past century (Lougheed et al., 2004). Emergent vegetation loss has been attributed to sustained high water levels in Lake Ontario over the past 30 years and physical destruction by carp, whereas the loss of submergent vegetation has been associated with the decreased water clarity due to sediment resuspension from wind and carp activity, as well as excessive nutrient loading. The submersed vegetation is typically dominated by *Potamogeton pectinatus, P. foliosus*, *P.crispus*, and several other less common species, such as *Myriophyllum spicatum*, *Zannichellia palustris*, *Elodea canadensis* and *Ceratophyllum demersum* (Lougheed et al., 2004). Within the Cootes Paradise marsh, the boundary between the perennial emergent, mainly cattail (*Typha sp.*), and submergent vegetation is a function of the water cycle. Currently, virtually all emergent plant re-establishment has been through active planting efforts, but on-going challenges for their full recovery stem from lake level regulation and the smothering rafts of algae and debris (Theÿsmeÿer et al., 2016). For emergent seedling germination and subsequent shoreline stabilization to occur, a maximum summer water level of < 74.75 mean sea level is required, but this condition has been rarely met over the two decades. Meadow marsh is a priority habitat that is used as an environmental indicator for Lake Ontario water level regulation. Although much of the potential meadow zone is vegetated in Cootes Paradise marsh, the plant community present is almost entirely non-native and thus not of useful character to most insect and wildlife species. Two highly aggressive non-native plant species dominate the local meadow marsh areas, common reed (*Phragmites australis)* and Eurasian manna grass *(Glyceria maxima)*, although the presence of the former species has been effectively managed (Theÿsmeÿer et al., 2016).

To reproduce the dynamics of the macrophyte community in Cootes Paradise, we first reviewed the pertinent literature and distinguished between processes that have been considered and others that are underrepresented by the current generation of aquatic mechanistic models

(Table 1). Past research has extensively focused on macrophyte growth limitations associated with light (Domin et al., 2004; Herb and Stefan, 2003; Herb and Stefan, 2006; Ikusima, 1970; Zimmerman et al., 1994), nutrients (Anderson et al., 1997; Plus et al., 2003; Wade et al., 2002a, 2002b), and oxygen (Park and Uchrin, 1997). Several studies have also reported light limitation associated with phytoplankton self-shading (Asaeda and Van Bon, 1997), epiphyte light inhibition (Wade et al., 2002a, 2002b), and invasive *Myriophyllum* light-shading (Miller et al., 2011). Except from these processes, there are at least two facets of the broader role of macrophytes that could be potentially considered in the next iteration of *WEM*, such as (*i*) allelopathy of submerged macrophytes to phytoplankton growth (Mulderij et al., 2007), and (*ii*) the refuge effect of submerged macrophytes to zooplankton (Li et al., 2010; Lv et al., 2016). However, given the lack of clear evidence of allelopathy in Cootes Paradise marsh and insufficient available data for zooplankton, both processes are not currently considered.

Rather than using the sophisticated modelling approach adopted by Asaeda et al. (2000), where macrophyte growth and decay processes are analyzed in different plant parts (shoots, roots, and tubers), *WEM* simplifies these metabolic processes and instead focuses on the competition patterns of the dominant macrophyte functional groups present in Cootes Paradise. Namely, based on the formulations of Kim et al. (2013, 2016), we distinguish among three macrophyte functional groups: meadow, emergent, and submerged plants. Similar to the phytoplankton governing equations, macrophyte growth was modulated by nutrient, temperature and light availability. Importantly, there are four key differences between macrophyte and phytoplankton processes with respect to resource (light and nutrient) procurement. First, photosynthesis by meadow and emergent plants is not limited by light availability at different water depths, whereas submerged plants, like phytoplankton, are strongly impacted by light attenuation and exhibit an inverse relationship with water depth. Second, meadows and emergent macrophytes exert light-shading effects on submerged macrophytes as well as on phytoplankton growth. The shading effect is assumed to increase with the areal coverage of meadows and emergent macrophytes, and is set to a maximum light reduction of 83% based on empirical evidence from Köhler et al. (2010). Third, *WEM* simulates macrophytes to uptake both DP_w and DP_{sd}, with an uptake ratio that varies based on the corresponding concentration variability (Granéli and Solander, 1988; Christiansen et al., 2016; see also Tables S1 and S2). Lastly, phosphorus retention in macrophyte tissues was based on the assumption that half of phosphorus taken up by macrophytes is rapidly released through respiration, while the other half is released through slow decomposition of dead plant tissues (Asaeda et al., 2000).

2.5. Sensitivity analysis

We used Monte-Carlo (*MC*) simulations of key input parameters to examine the *WEM* ability to reproduce the interplay among phytoplankton, macrophytes, and sediment nutrient release in Cootes Paradise. Two different strategies of sensitivity analysis were then implemented: multiple-linear regression and the pattern recognition algorithm, Self-Organizing Maps (*SOM*s).

2.5.1. Multiple-linear regression

Multiple-linear regression evaluated the variability of model outputs induced by perturbations of selected inputs (external nutrient loading and model parameters). Namely, five external loading sources were selected, *WWTP*, *CSO*s, and three tributaries (i.e., Spencer, Chedoke and Borer's creeks), along with a total of forty-eight (48) model parameters related to the dynamics of macrophytes and phytoplankton, and the characterization of sediment processes. The magnitude of input perturbations for *MC* simulations was pre-specified within the ± 30% and ± 15% ranges for the default values of external forcing and model parameters, respectively. We then used Latin Hypercube sampling to independently generate 3×5000 input vectors. We developed multiple-linear regression models based on the following inputs: (*i*) external TP loading, (*ii*) the selected subset of model parameters, and (*iii*) both of these inputs (referred to as a "combined exercise" hereafter). Response variables to evaluate model sensitivity were the predicted averages of *TP*, Chl*a* and submerged macrophyte biomass during the growing season (May to October). Model inputs were ranked with respect to their influence on these model endpoints according to the respective squared semi-partial correlation coefficients (r^2_{sp}).

2.5.2. Projection of non-linear ecological relationships using Self-Organizing Maps

The former method of sensitivity analysis is conceptually straightforward and statistically robust but is not designed to capture non-linear relationships between model endpoints and individual ecological mechanisms or external forcing factors. To address this weakness, we used Self-Organizing Maps; an un-supervised pattern-recognition algorithm based on artificial neural networks. This approach has been recognized as a powerful means for extracting information from complex multi-dimensional data in ecology (Chon, 2011). *SOM* visually describes relationships between multivariate data onto 2-D maps by adaptively computing similarities among multi-dimensional vectors, and provides more flexibility to analyze non-linear dependencies in complex systems, compared to the limitations of linear statistical tools, such as Principal Component Analysis (Frey and Rusch, 2013; Giraudel and Lek, 2001; Kohonen, 2001). Thus, the rationale of our *SOM* application to sensitivity analysis is that conventional linear regression may not adequately account for the complex ecological interplay among system elements represented by *WEM*. In particular, our working hypothesis is that the causal relationships associated with an abrupt, non-linear shift from the clear-macrophyte dominant state to the turbid-phytoplankton dominant state in Cootes Paradise marsh, may be more effectively captured through the use of *SOM*.

SOM consists of two layers, which are referred to as input and output vectors/neurons. In addition to these neurons, the virtual connectivity between input and output layers is defined as weight vectors (also known as codebook neurons). During the data-training phase, the distances between input and weight vectors/neurons are estimated. The best matching unit (*BMU*) is designated as the weight vector that has the shortest distance to the input vector. Subsequently, all the weight vectors are updated and adjusted according to topology of the *BMU*, until they become stabilized over time. During this data-training process in which the non-linear projection is formed, all neighbouring weight vectors resemble to each other in similar topography (the so-called a local relaxation or smoothing effect, see pp. 109–115 in Chapter 3, Kohonen, 1997). The primary mathematical formulas of *SOM* are expressed as follows:

$$|x - \omega_{BMU}| = \min_i |x - \omega_i|$$

$$\omega_i(t+1) = \omega_i(t) + h(t) \cdot d_i(t)$$

$$h(t) = \alpha(t) \cdot \exp\left(-\frac{|\omega_{BMU} - \omega_i|^2}{2\sigma^2(t)}\right)$$

where $d_i(t)$ represents a minimum Euclidean distance between input x and weight ω in the i number of individual nodes (i.e., identical to the *SOM* size) at time t. The neighbourhood function $h(t)$ plays a pivotal role as a smoothing kernel defined over the *SOM* hexagonal lattices. For convergence, $h(t) \to 0$ while time $t \to \infty$; both the learning-rate factor $\alpha(t)$ and the *BMU*-coverage width $\sigma^2(t)$ are monotonically decreasing over time.

The *SOM* is implemented using a non-commercialized toolbox developed by the Helsinki University of Technology (Vesanto et al., 2000). Based on the aforementioned *MC* runs, we selected 40 input variables for our *SOM* analysis. In this study, the data ordination is mapped onto a hexagonal cell grid, whereby similar individual vectors of each *MC*

run occupy adjacent cells during the *SOM* training phase. The 40 input variables (i.e., individual vectors) consist of 14 model parameters, four external forcing functions, 10 state variables from the model, and 12 daily total phosphorus flux values. Here, we opted for a *SOM* size equal to 364 cells, which is close to the recommendation, $5\sqrt{\text{sample size}}$, of Vesanto and Alhoniemi (2000). Regarding the map shape, we optimized it (26 × 14 cells) by considering minimization of both quantization and topological errors (Park et al., 2014). The initial weight neurons were randomized using the greatest eigenvector of covariance matrix of dataset. After ordination of the data by *SOM*, we applied an additional cluster analysis using the final weight neurons and then summarized the dominant patterns quantitatively with the U-matrix (Cuddington et al., 2013; Kohonen, 2001; Wroblewski, 1980). To characterize the dominant ecological features of Cootes Paradise, we compared the average values of input variables in each cluster. Results from *SOM* analysis were then evaluated against those obtained from conventional multiple-linear regression analysis.

3. Results

3.1. WEM sensitivity analysis with linear regression

The first sensitivity analysis exercise considered only the external *TP* loading sources from Dundas *WWTP*, local *CSO*s, and three major tributaries to evaluate their relative importance to Cootes Paradise marsh. The coefficients of determination values for *TP*, Chl*α* concentrations and submerged macrophyte biomass were very high ($r^2 \approx 0.99$), which indicates that the relationship between nutrient inflows and model outputs can be approximated as linear and the system does not reach its carrying capacity, nor does it experience a distinct shift into an alternative state, within the selected layout (i.e., magnitude of the nutrient loading perturbations induced, seasonal averaging of model endpoints) (Table 3). Our analysis primarily shows that the dynamics of Cootes Paradise marsh are significantly influenced by the loading from Spencer (TP_{SPN}) and Chedoke (TP_{CHE}) creeks. In particular, the corresponding squared semi-partial correlation coefficient (r^2_{sp}) values accounted for 45–53% and 17–19% of the variability of the ambient *TP* concentrations. Conversely, the impact of *TP* loading from Borer's Creek is negligible (< 1%). Given the similar catchment size and hydraulic loading from Chedoke (24.9 km^2) and Borer's (19.8 km^2) creeks, we can infer that the urbanized Chedoke Creek is responsible for significantly higher *TP* areal export than the agricultural Borer's Creek. This finding contradicts the popular notion that agricultural lands display greater propensity for *TP* export relative to urbanized locations (Moore et al., 2004; Soldat and Petrovic, 2008), but is consistent with several studies conducted in Southern Ontario that have provided evidence in support of the opposite pattern (Kim et al., 2017; Wellen et al., 2014a; Winter and Duthie, 2000). Likewise, Theÿsmeÿer et al. (2009) noted that the smaller Chedoke creek was responsible for approximately four-fold higher areal *TP* loading than the larger, predominantly agricultural watershed drained by Spencer creek. Nevertheless, it is important to further elucidate the role of Spencer and Borer's creeks, given that Wellen et al. (2014b) highlighted the greater uncertainty (including year-to-year variability) of the hydraulic loading and *TP* export estimates from the agricultural sites in the area. *WWTP* effluent discharge and *CSO*s accounted for 18–23% and 12–14% variability of the ambient *TP* concentrations in Cootes Paradise marsh, respectively. However, if we consider that our study period does not consider the upgrades of the Dundas *WWTP* in 2013 to lower *TP* concentrations in effluent and practically eliminate the discharges from *CSO*s, it is reasonable to infer that the role of non-point source loading from the local tributaries may be even more predominant than what is shown by the present sensitivity exercise.

The second sensitivity analysis exercise, involving 48 model parameters, resulted in multiple regression models with distinctly lower r^2 values (0.63–0.84). Interestingly, some of the most influential parameters were associated with the characterization of the sediment and macrophyte dynamics (Table 4). Ambient *TP* is strongly influenced by the specification of sediment porosity (φ), which contributes 45% of the predicted variability in Cootes Paradise marsh. This result suggests that sediment porosity affects interstitial water content, or the degree of phosphorus dilution in the pore water, which in turn directly influences the diffusive reflux from sediments to the water column. Considering that *TP* has been strongly correlated with phytoplankton in Cootes Paradise (Thomasen and Chow-Fraser, 2012), the signature of sediment porosity is also evident on Chl*α* concentrations, albeit much weaker than the one registered from the optimal temperature ($T_{opt(j=MDW,EMG)}$) for meadow and emergent macrophyte growth (Table 4). The same result holds true for submerged macrophyte biomass, and thus $T_{opt(j=MDW,EMG)}$ accounts for 71% and 36% of variability of the

Table 3
WEM sensitivity analysis using multiple-regression modelling. Coefficient of determination (r^2) values for three predicted outputs, seasonal (May–October) average values of *TP*, Chl*α* and submerged macrophyte biomass, are provided in the corresponding subheadings (N = 5000). Model input ranking is based on the squared semi-partial correlation coefficient (r^2_{sp}).

	TP	r^2_{sp}	*Chlα*	r^2_{sp}	*Submerged Macrophytes*	r^2_{sp}
External forcing functions**	r^2 = 0.99		r^2 = 0.99		r^2 = 0.99	
	TP_{SPN}	0.46	TP_{SPN}	0.53	TP_{SPN}	0.45*
	TP_{WTP}	0.2	TP_{WTP}	0.18	TP_{WTP}	0.23*
	TP_{CHE}	0.19	TP_{CHE}	0.17	TP_{CSO}	0.17*
	TP_{CSO}	0.14	TP_{CSO}	0.12	TP_{CHE}	0.13*
	TP_{BOR}	< 0.01	TP_{BOR}	< 0.01	TP_{BOR}	< 0.01*
Parameters	r^2 = 0.83		r^2 = 0.84		r^2 = 0.63	
	φ	0.45*	$T_{opt(j=MDW,EMG)}$	0.71	$T_{opt(j=MDW,EMG)}$	0.36*
	$T_{opt(j=MDW,EMG)}$	0.09	φ	0.04*	$\Psi_{Pup(j=SUB)}$	0.05
	v_{sett}	0.07*	$I_{opt(i)}$	0.02*	$\omega G_{(j=MDW)}$	0.05
	$\omega_{Dcp(k=G2)}$	0.06	$KP_{(i=A)}$	0.01*	$I_{opt(j=SUB)}$	0.04*
	ω_{rs}	0.05	$\omega G_{(i=B)}$	0.01	$\omega R_{(j=SUB)}$	0.03*
Combined exercise	r^2 = 0.93		r^2 = 0.92		r^2 = 0.80	
	φ	0.30*	$T_{opt(j=MDW,EMG)}$	0.77	$T_{opt(j=MDW,EMG)}$	0.45*
	TP_{SPN}	0.15	φ	0.05*	$\omega G_{(j=MDW)}$	0.09
	TP_{WTP}	0.07	$\omega G_{(j=EMG)}$	0.01*	$T_{opt(j=SUB)}$	0.07*
	TP_{CHE}	0.07	$\omega_{Dcp(k=G2)}$	0.01*	ω_{rs}	0.01*
	$T_{opt(j=MDW,EMG)}$	0.06	$KP_{(i=A)}$	< 0.01	$I_{opt(i)}$	0.01*

* Negative sign of the corresponding regression coefficient.
** Abbreviations related to external forcing functions denote *TP* loading from Spencer ($_{SPN}$), Chedoke ($_{CHE}$), Borer's ($_{BOR}$) creeks, Dundas wastewater treatment plant ($_{WTP}$), and combined sewer overflows ($_{CSO}$), respectively.

Table 4
Sensitivity analysis using Self-Organizing Maps. Bolded numbers indicate the highest value registered among all clusters for each model state variable, *P* flux, model parameter, and external loading forcing function.

Variables	*Units*	Mean	Cluster 1*	Cluster 2	Cluster 3	Cluster 4	Cluster 5
Chlα	$\mu g{\cdot}L^{-1}$	43.49	**60.78^{e}**	28.54^{b}	52.21^{d}	32.86^{c}	27.82^{a}
TP	$\mu g{\cdot}L^{-1}$	143.4	**155.0^{e}**	149.2^{d}	139.6^{c}	132.4^{a}	136.4^{b}
$cMAC_{\partial}j_{=SUB)}$	$g{\cdot}m^{-2}$	37.10	7.19^{b}	68.48^{d}	4.68^{a}	35.48^{c}	**97.57^{e}**
$cMAC_{\partial}j_{=MDW)}$	$g{\cdot}m^{-2}$	318	20^{a}	153^{c}	28^{b}	401^{d}	**1187^{e}**
$cMAC_{\partial}j_{=EMG)}$	$g{\cdot}m^{-2}$	256	17^{b}	**1085^{e}**	5^{a}	211^{c}	290^{d}
cDP_{w}	$\mu g{\cdot}L^{-1}$	23.84	23.38^{b}	25.99^{d}	19.42^{a}	24.28^{c}	**28.45^{e}**
cPP_{w}	$\mu g{\cdot}L^{-1}$	75.61	69.57^{b}	**93.60^{e}**	69.24^{a}	75.00^{c}	78.44^{d}
cDP_{sd}	$\mu g{\cdot}L^{-1}$	1119	**2114^{e}**	485^{a}	1236^{d}	558^{c}	527^{b}
$cPP_{(k)}$	$g{\cdot}kg^{-1}$	1.534	1.407^{b}	1.699^{d}	1.406^{a}	1.581^{c}	**1.716^{e}**
kext	m^{-1}	6.633	**7.682^{e}**	5.680^{b}	6.875^{d}	5.656^{a}	6.348^{c}
DP_{Dif}	$kg{\cdot}day^{-1}$	3.89	**7.31^{e}**	1.73^{a}	4.27^{d}	1.93^{c}	1.87^{b}
$DP_{sdUp(j)}$	$kg{\cdot}day^{-1}$	4.928	0.394^{b}	**12.85^{e}**	0.257^{a}	4.996^{c}	11.01^{d}
$DP_{wM(i)}$	$kg{\cdot}day^{-1}$	1.71	1.78^{d}	**1.96^{e}**	1.47^{a}	1.73^{c}	1.72^{b}
$DP_{wR(j)}$	$kg{\cdot}day^{-1}$	0.199	0.016^{b}	**0.823^{e}**	0.004^{a}	0.163^{c}	0.236^{d}
$DP_{wUP(i)}$	$kg{\cdot}day^{-1}$	12.38	**15.95^{e}**	10.12^{b}	13.37^{d}	10.38^{c}	9.44^{a}
$DP_{wUp(j)}$	$kg{\cdot}day^{-1}$	0.211	0.002^{b}	**0.945^{e}**	0.0002^{a}	0.134^{c}	0.250^{d}
$P_{Sett(i)}$	$kg{\cdot}day^{-1}$	2.69	**3.35^{e}**	2.34^{c}	2.84^{d}	2.32^{b}	2.14^{a}
$PP_{rs(k)}$	$kg{\cdot}day^{-1}$	7.55	7.05^{b}	8.16^{d}	6.99^{a}	7.84^{c}	**8.28^{e}**
PP_{Sett}	$kg{\cdot}day^{-1}$	4.83	4.49^{b}	**6.03^{e}**	4.40^{a}	4.64^{c}	5.04^{d}
$PP_{sdM(k)}$	$kg{\cdot}day^{-1}$	0.742	0.056^{b}	**2.034^{e}**	0.036^{a}	0.735^{c}	1.598^{d}
$PP_{wM(i)}$	$kg{\cdot}day^{-1}$	1.14	1.19^{d}	**1.30^{e}**	0.98^{a}	1.16^{c}	1.15^{b}
$PP_{wR(j)}$	$kg{\cdot}day^{-1}$	1.129	0.093^{b}	**4.663^{e}**	0.027^{a}	0.928^{c}	1.340^{d}
$\omega G_{(j=SUB)}$	day^{-1}	0.060	0.060^{b}	0.060^{b}	0.060^{b}	0.059^{a}	**0.061^{c}**
$\omega G_{(j=EMG)}$	day^{-1}	0.060	0.059^{a}	**0.062^{c}**	0.059^{a}	0.060^{b}	0.059^{a}
$\omega G_{(j=MDW)}$	day^{-1}	0.060	0.059^{a}	0.059^{a}	0.060^{b}	**0.061^{c}**	**0.061^{c}**
$\omega R_{(j=EMG)}$	day^{-1}	0.019	0.019^{b}	0.019^{b}	0.019^{b}	0.019^{b}	0.0187^{a}
$\omega R_{(j=MDW)}$	day^{-1}	0.019	0.019^{b}	0.018^{a}	0.019^{b}	0.019^{b}	**0.019^{b}**
$\omega_{Dcp(k=G2)}$	day^{-1}	1.0×10^{-4}	1.02×10^{-4d}	**1.04×10^{-4e}**	0.98×10^{-4b}	0.95×10^{-4a}	1.01×10^{-4c}
ω_{rs}	day^{-1}	3.5×10^{-4}	3.5×10^{-4}	3.5×10^{-4}	3.5×10^{-4}	**3.6×10^{-4}**	3.5×10^{-4}
$I_{opt(i)}$	$MJ{\cdot}m^{-2}{\cdot}day^{-1}$	10.01	9.96	9.97	10.02	**10.21**	9.95
$I_{opt(j=SUB)}$	$MJ{\cdot}m^{-2}{\cdot}day^{-1}$	14.96	14.81^{b}	15.02^{c}	15.16^{d}	**15.70^{e}**	14.31^{a}
$KP_{(i=A)}$	$\mu g{\cdot}L^{-1}$	13.02	**13.31^{e}**	13.14^{c}	12.74^{a}	13.18^{d}	12.79^{b}
$\Psi_{Pup(j=SUB)}$	–	0.080	0.080^{c}	0.080^{c}	0.079^{b}	0.078^{a}	**0.082^{d}**
$T_{opt(j=EMG,MDW)}$	°C	24.96	28.35^{d}	20.60^{a}	**28.54^{e}**	22.56^{c}	20.70^{b}
v_{sett}	$m{\cdot}day^{-1}$	0.0299	0.0301^{c}	**0.0305^{e}**	0.0296^{b}	0.0290^{a}	0.0302^{d}
φ	%	85.048	81.075^{a}	82.456^{b}	88.629^{d}	**89.070^{e}**	84.734^{c}
TP_{SPN}	$kg{\cdot}day^{-1}$	10.57	10.58^{c}	**10.69^{e}**	10.64^{d}	10.32^{a}	10.56^{b}
TP_{WTP}	$kg{\cdot}day^{-1}$	6.094	6.077	**6.128**	6.092	6.099	6.087
TP_{CSO}	$kg{\cdot}day^{-1}$	4.450	4.402	4.496	4.462	4.390	**4.504**
TP_{CHE}	$kg{\cdot}day^{-1}$	4.410	4.356^{b}	**4.540^{e}**	4.441^{d}	4.333^{a}	4.393^{c}

* Superscript letters indicate cluster similarity based on Scheffé's test. Lack of superscript letters show no statistically significant difference among the five clusters.

predicted Chl*α* concentrations and submerged macrophyte biomass in the marsh, respectively. It is also worth noting the opposite signs of the two relationships along with the fact Chl*α* concentrations appear to be more sensitive to a macrophyte- ($T_{opt(j=MDW,EMG)}$) rather than phytoplankton-related parameters ($I_{opt(i)}$, $KP_{(i=B)}$, and $\omega G_{(i=B)}$). The negative relationship between optimal temperature for meadow/emergent macrophyte growth and submerged vegetation abundance seems somewhat counterintuitive and reflects the coexistence patterns within the simulated macrophyte assemblage as well as the competition forces with phytoplankton. Given the prevailing water temperatures in Cootes Paradise marsh, the assumption of higher optimal temperature ($T_{opt(j=MDW,EMG)}$) renders slower meadow and emergent macrophyte growth rates, but the submerged vegetation does not appear to capitalize upon the release from the competition with the other two simulated macrophyte functional groups. In particular, the positive relationship between Chl*α* concentrations and $T_{opt(j=MDW,EMG)}$ suggests that phytoplankton outcompetes the submerged macrophytes under the nutrient-enriched and light-limiting conditions currently prevailing in the water column of Cootes Paradise marsh (Bolpagni et al., 2014; Dong et al., 2015; Kurtz et al., 2003). Indicative of the inadequate light availability for submerged macrophyte growth in Cootes Paradise marsh is the fact that the predicted abundance is not particularly sensitive even on the values assigned to their optimal light intensity (I_{optSUB}) (r^2_{sp} = 0.04). This pattern is conceptually on par with the widespread decline of submerged vegetation in coastal wetlands around the Great Lakes, predominantly induced by cultural eutrophication and excessive phytoplankton growth (McNair and Chow-Fraser, 2003).

Finally, the third sensitivity analysis exercise aimed to examine the interplay between external loading and ecological processes considered by the model. We found that ambient *TP* is more strongly influenced by φ, which explains an approximately equal amount of the associated variability (30%) with the collective impact of the loading from Spencer Creek, Dundas *WWTP*, and Chedoke Creek (Table 4). For both Chl*α* and submerged macrophyte biomass, $T_{opt(j=MDW,EMG)}$ was again the most influential parameter and the corresponding squared semi-partial correlation coefficients were increased by 6–9% (Table 4). Paradoxically, a suite of parameters associated with the characterization of potentially important physiological or biogeochemical processes, such as the kinetics of phosphorus uptake from individual phytoplankton groups ($KP_{(i=A)}$), maximum gross photosynthesis rate of emergent and meadow macrophytes ($\omega G_{(j=EMG/MDW)}$), sediment decomposition rate for refractory phosphorus, ($\omega_{Dcp(k=G2)}$), and sediment resuspension rate (ω_{rs}), appear to exert control over the predictions of key model endpoints, but their magnitude suggests a secondary role in modulating the interplay among phytoplankton, macrophytes, and nutrient sediment release in the studied eutrophic wetland. Given that the residual variability of the linear models varies from 7% to 37% (Table 4), when ecological parameters are considered with our Monte Carlo simulations, the next step of the study examined to what extent a method designed to elucidate complex non-linear dynamics is more suitable to identify

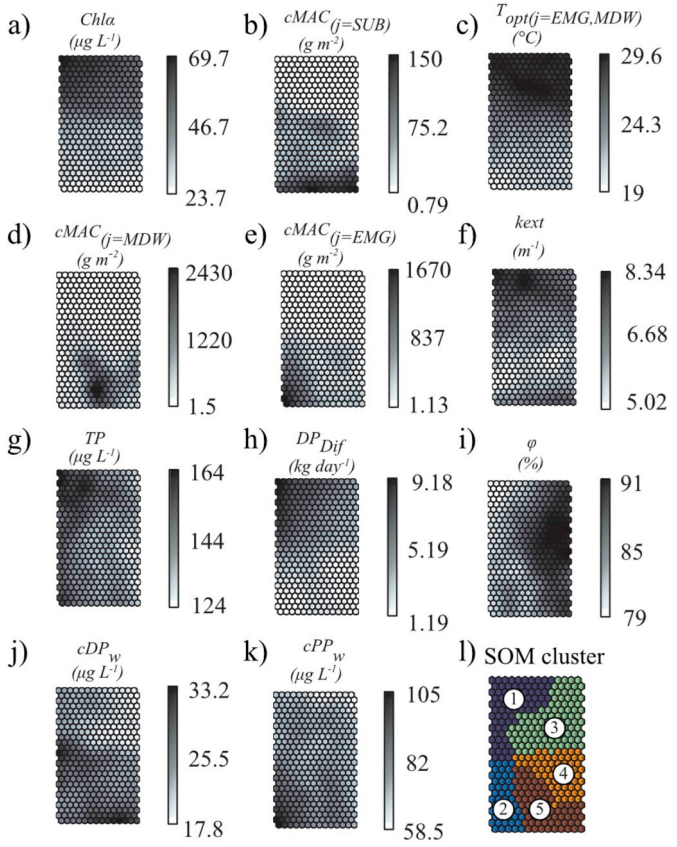

Fig. 3. Self Organizing Map (*SOM*) outputs for (*a*) Chlorophyll α concentrations, (*b*) submerged macrophyte biomass, (*c*) optimal temperature for meadow and emergent macrophyte vegetation, (*d*) meadow macrophyte biomass, (*e*) emergent macrophyte biomass, (*f*) light extinction coefficient, (*g*) total phosphorus in the water column, (*h*) dissolved phosphorus diffusion from the sediment, (*i*) sediment porosity, (*j*) dissolved phosphorus concentrations in the water column, (*k*) particulate phosphorus concentrations in the water column, and (*l*) the five *SOM* clusters.

model sensitivity patterns for a eutrophic wetland (Herb and Stefan, 2003; Li et al., 2010; Lv et al., 2016; Mulderij et al., 2007).

3.2. WEM sensitivity analysis with Self-Organizing Maps

SOM produces colour-gradient maps for each of the 40 model state variables, *P* fluxes, model parameters, and external loading forcing functions considered, whereby we can understand the various interrelationships by comparing the gradient maps vis-à-vis the identified homogeneous clusters (Figs. 3 and S1). For instance, Chl*α* displays the darkest colour hexagonals at the upper part of *SOM* (Fig. 3a). This pattern corresponds to Clusters 1 and 3 (Fig. 3l). In contrast, dark grey regions with submerged macrophytes mainly appear at the bottom part of *SOM* (Fig. 3b), which correspond to Clusters 2 and 5 (Fig. 3l). This contrasting pattern reflects an inverse relationship between Chl*α* concentration and submerged macrophyte abundance. Similar to Chl*α*, the highest values of $T_{opt(j=MDW,EMG)}$ is located at the upper part of *SOM* (Fig. 3c). This pattern reinforces our previous explanation that higher $T_{opt(j=MDW,EMG)}$ values accentuate the temperature limitations on plant growth, thereby leading to lower meadow and emergent biomass (Figs. 3d–e). Nonetheless, the submerged vegetation does not benefit from this handicap of the other two residents of the simulated macrophyte assemblage, and thus the resource competition in the water column appears to favour phytoplankton. The latter pattern invites further investigation, given that submerged macrophytes can uptake nutrients from two pathways (sediments and water column) and thus presumably possess a competitive advantage over phytoplankton. One plausible explanation can be sought from the *SOM* derived for the light-attenuation coefficient (see *Kext* in Fig. 3f), which draws parallels with the one derived for Chl*α* concentrations and is in direct contrast to the one for submerged macrophyte biomass (Fig. 3b). This relationship reflects the popular notion that submerged macrophytes are particularly susceptible to light limitation relative to phytoplankton. Phytoplankton may be more effective in adapting to both low intensity and quality of light by increasing the size and/or number of photosynthetic units. Both strategies maximize the likelihood to capture light photons and ultimately transfer light energy to reaction centers (Falkowski and Owens, 1980). Additionally, although this effect is not explicitly considered by our model, the shading effects from periphyton (complex community of organisms such as algae, bacteria, fungi, and detritus attached to submerged macrophytes) may serve as another plausible explanation for the greater sensitivity to light attenuation displayed by submerged macrophytes (Granéli and Solander, 1988; Raeder et al., 2010). Earlier work from Sand-Jensen and Borum (1984) has showed that macrophytes (i.e, the stoloniferous *Lobelia dortmanna*) can be heavily shaded by epiphytes even in clear-water lakes, limiting their depth penetration to 1.0 m, instead of 3.5 m without epiphytes.

Regarding the depicted nature of the *TP*-Chl*α* relationship from *WEM*, the *SOM* analysis offered interesting insights. Although the highest average *TP* and Chl*α* values are classified in Cluster 1, the second highest *TP* and Chl*α* concentrations are found in Clusters 2 and 3, respectively (Table 4). The similarities among *TP* (Fig. 3g), Chl*α* concentrations and sediment diffusive reflux (DP_{Dif}) in the *SOM* patterns (Fig. 3h) suggest that the *TP*-Chl*α* relationship is tighter under elevated reflux rates of biologically available phosphorus in the water column. This *SOM* pattern is also consistent with our earlier result that *TP* is most sensitive to sediment porosity (*φ*) (Fig. 3i), which is regarded as one of the main factors that determines nutrient dilution in interstitial waters and thus the magnitude of Fickian diffusive transport. *SOM* also shows that dissolved phosphorus (cDP_w) decreases when Chl*α* increases (Fig. 3j), which reflects the ability of phytoplankton to modulate ambient cDP_w levels through uptake. Interestingly, moderate resemblance exists between the *SOM* for *TP* and the one derived for particulate *P* concentrations in the water column (cPP_w) (Fig. 3j). The interplay among phytoplankton, macrophytes, and sediment diagenesis is generally characterized by five *SOM* clusters (Fig. 3l), each of which represents a distinct state of the ecosystem (Table 4). Cluster 1 is characterized by high *TP* and Chl*α* concentrations, high phosphorus uptake rates by phytoplankton ($P_{UP(i)}$), high dissolved phosphorus in the sediment pore water (DP_{sd}), as well as diffusive reflux rate (DP_{Dif}). The same cluster is also characterized by high background light attenuation, *kext*. Cluster 2 is characterized by the predominance of macrophytes, particularly emergent and less so submerged vegetation, whereas the Chl*α* concentrations are significantly reduced. Interestingly, the internal phosphorus flux rates (PP_{wSett}, DP_{wM}, DP_{sdUp}, DP_{wUp}, DP_{wR}, and PP_R,) are approximately two to three times higher than average in Cluster 2 (Table 5). The same cluster is also characterized by high external loading fluxes from Spencer and Chedoke creeks or the Dundas *WWTP*, which in turn replenish the sediment pool and establish an active positive feedback loop, thereby allowing for the acceleration of phosphorus recycling rates and persistently high ambient *TP* concentrations in the wetland. In Cluster 3, excessively high optimal growth temperature $T_{opt(j=MDW,EMG)}$ may adversely affect the proliferation of meadow and emergent plants (as previously discussed), which leads to the second and third highest average Chl*α* and *TP* concentrations among the five clusters, respectively. The same cluster is also associated with the second highest light attenuation, *kext*, as well as sediment porosity *φ*. Additionally, although lower than average (43.49 μg L^{-1}), Chl*α* concentrations in Cluster 4 are relatively high (32.86 μg L^{-1}) considering the somewhat lower external phosphorus loading (Table 4). A plausible explanation for this result may be that macrophyte biomass is not high enough to outcompete phytoplankton

Table 5
WEM sensitivity analysis using Self-Organizing Maps. Model input ranking is based on their squared semi-partial correlation coefficient (r^2_{sp}) against the seasonal (May–October) average values for ambient TP, Chlα and submerged macrophyte biomass.

	Cluster 1	r^2_{sp}	Cluster 2	r^2_{sp}	Cluster 3	r^2_{sp}	Cluster 4	r^2_{sp}	Cluster 5	r^2_{sp}
TP	φ	0.24	φ	*0.23*	TP_{SPN}	0.25	TP_{SPN}	0.30	TP_{SPN}	0.19
	TP_{SPN}	0.22	TP_{SPN}	*0.21*	φ	0.22	TP_{WTP}	0.14	φ	0.11
	$\omega_{Dcp(k=G2)}$	0.10	$\omega_{Dcp(k=G2)}$	*0.14*	TP_{CHE}	0.10	TP_{CHE}	0.13	TP_{WTP}	0.09
	TP_{CHE}	0.10	v_{sett}	*0.10*	TP_{WTP}	0.10	φ	0.10	TP_{CHE}	0.09
	TP_{WTP}	0.10	TP_{WTP}	*0.09*	TP_{CSO}	0.07	v_{sett}	0.09	$\omega G_{(j=MDW)}$	0.08
Chlα	$T_{opt(j=MDW,EMG)}$	0.39	$T_{opt(j=MDW,EMG)}$	*0.31*	$T_{opt(j=MDW,EMG)}$	0.30	$T_{opt(j=MDW,EMG)}$	0.49	$T_{opt(j=MDW,EMG)}$	0.32
	φ	0.12	$I_{opt(j=SUB)}$	*0.12*	φ	0.24	$\omega G_{(j=EMG)}$	0.09	$I_{opt(j=SUB)}$	0.16
	$\omega_{Dcp(k=G2)}$	0.06	$\omega G_{(j=SUB)}$	*0.09*	$KP_{(i=A)}$	0.10	$\omega R_{(j=MDW)}$	0.06	$\omega G_{(j=SUB)}$	0.13
	$KP_{(i=A)}$	0.03	$\Psi_{Pup(j=SUB)}$	*0.07*	$\omega_{Dcp(k=G2)}$	0.05	$\Psi_{Pup(j=SUB)}$	0.06	$\Psi_{Pup(j=SUB)}$	0.10
	ω_{rs}	< 0.01	$I_{opt(i)}$	*0.06*	ω_{rs}	0.04	$\omega G_{(j=SUB)}$	0.03	$\omega G_{(j=EMG)}$	0.02
Submerged macrophyte biomass	$T_{opt(j=MDW,EMG)}$	0.16	$I_{opt(j=SUB)}$	*0.21*	$T_{opt(j=MDW,EMG)}$	0.13	$\Psi_{Pup(j=SUB)}$	0.28	$I_{opt(j=SUB)}$	0.22
	$\Psi_{Pup(j=SUB)}$	0.05	$\omega G_{(j=SUB)}$	*0.21*	$\Psi_{Pup(j=SUB)}$	0.04	$\omega G_{(j=SUB)}$	0.19	$\omega G_{(j=SUB)}$	0.21
	$\omega G_{(j=SUB)}$	0.02	$\Psi_{Pup(j=SUB)}$	*0.20*	$\omega G_{(j=SUB)}$	0.02	$I_{opt(j=SUB)}$	0.10	$\Psi_{Pup(j=SUB)}$	0.18
	$I_{opt(j=SUB)}$	0.02	$T_{opt(j=MDW,EMG)}$	*0.08*	$KP_{(i=A)}$	0.02	$T_{opt(j=MDW,EMG)}$	0.06	$T_{opt(j=MDW,EMG)}$	0.11
	ω_{rs}	0.01	$\omega G_{(j=EMG)}$	*0.04*	TP_{SPN}	0.01	ω_{rs}	0.04	$I_{opt(i)}$	0.03

in Cootes Paradise marsh. This assertion is also reinforced by the high porosity, φ, levels (89.07%), the fairly sediment P concentrations, cDP_{sd}, (558 μg P L^{-1}), and the fairly low macrophyte phosphorus uptake, DP_{sdUp}, (4.99 kg P d^{-1}) characterizing the same cluster. Interestingly, Cluster 4 is also associated with relatively low optimal temperature for meadow and emergent macrophyte growth, $T_{opt(j=MDW,EMG)}$, which in turn explains their relatively high abundance levels. Cluster 5 is marked by high biomass levels of submerged and meadow macrophytes, triggered by their relatively high growth rates assigned. In the same cluster, Chl*α* and *TP* concentrations display lower than average values, partly associated with a weak internal nutrient recycling loop. Interestingly, the sediment resuspension fluxes ($PP_{rs(k)}$) cannot compensate for the latter pattern, even though Cluster 5 is characterized by its highest value among the five clusters.

As a final step, we conducted a multiple-linear regression analysis with the same response and predictor variables within each of the five clusters extracted from our *SOM* analysis (Table 5). Similar to our original results, ambient *TP* levels are sensitive to the specification of the sediment porosity (φ) in Cootes Paradise marsh, but the external loading from Spencer Creek (TP_{SPN}) appears to be equally influential across all the clusters. Other factors ranked highly in shaping the *TP* concentrations were the loading from the Dundas wastewater treatment plant (TP_{WTP}), the Chedoke Creek (TP_{CHE}), as well as the decomposition rate for labile phosphorus in the sediments ($\omega_{Dcp(k=G1)}$), and the settling rates of particulate phosphorus (v_{TSS}). Depending on the cluster considered, these sources and sinks of phosphorus are responsible for 55–75% of the predicted *TP* variability in the system. Consistent with our previous results, Chl*a* concentrations are predominantly influenced by the optimal temperature for emergent and meadow macrophyte growth rates ($T_{opt(j=MDW,EMG)}$), which can lead to a substantial reduction of their biomass and ultimately to the predominance of phytoplankton over the submerged vegetation. The nature of the latter competition is more clearly teased out with our *SOM* analysis, in that the ability of submerged macrophytes to exploit the available light underwater determines their ability to coexist or to be competitively excluded by phytoplankton. In particular, the optimal solar radiation for submerged macrophytes ($I_{opt(j=SUB)}$) is the most sensitive parameter to submerged macrophytes in Clusters 2 and 5, accounting for 21–22% and 12–16% of macrophyte and phytoplankton biomass variability, respectively (Table 5). In comparison, the importance of $I_{opt(j=SUB)}$ is not detected at all by the conventional linear regression analysis (see "combined exercise" in Table 3). The advantage of *SOM* analysis is also apparent through the elucidation of the importance of $\Psi_{Pup(j=SUB)}$ (i.e., phosphorus uptake fraction between sediment and water column) on submerged macrophyte biomass. Specifically, $\Psi_{Pup(j=SUB)}$ is the highest in Cluster 4 and accounts for 28% variability of submerged macrophyte biomass. Interestingly, two factors that could conceivably be important in shaping the phytoplankton-macrophyte competition, i.e., maximum gross photosynthesis rate of macrophytes ($\omega G_{(j=SUB)}$) and sediment resuspension rate (ω_{rs}), do not appear to drive > 2% of the submerged macrophyte variability.

On a final note, even though our *SOM* analysis delineated five clusters (or combinations of ecosystem conditions-external forcing-parameter values), the ranges of critical water quality indicators were not indicative of a distinct shift to an alternative improved state (TP > 130 μg L^{-1}, Chl*a* > 27 μg L^{-1}). In this regard, a subsequent exploratory analysis indicated that a critical factor to induce a non-linear regime shift to a clear submerged macrophyte-dominated state is the ability of submerged macrophytes to sequester phosphorus, as defined by the values assigned to their respiration and mortality rates, and P quotas in plant tissues. In particular, we found that a realistic 25% reduction in exogenous P loading (27.1 to 20.3 kg day^{-1}) coupled with a decrease of submerged macrophyte respiration (0.0165 to 0.0135 day^{-1}) and mortality (0.0528 to 0.0432 day^{-1}) rates, as well as an increase of the P quotas in plant tissues (0.0025 to 0.0125 g P g DW^{-1}) was sufficient to bring a distinct improvement in the prevailing water quality conditions (Fig. 4).

4. Discussion-Synthesis

Our study presented a process-based wetland model designed to reproduce the competition patterns among multiple phytoplankton and macrophyte functional groups, as modulated by the release of phosphorus from the sediments into the water column. Given its intended use, our primary focus was the characterization of the ecophysiological processes representing the nutrient uptake of the autotrophic assemblage from the water column and/or the sediment pore water, their relative ability to harvest light and fuel photosynthesis, as well as the temperature control of their growth and basal metabolism. Several key findings and lessons learned from this study are as follows:

- Our literature review showed a wealth of knowledge and a range of parameterizations with respect to the control of macrophyte growth from temperature, light, nutrient, and oxygen availability. Existing modelling efforts have also attempted to examine the light limitation posed by the shading from phytoplankton, epiphytes, or other invasive plant species. Some work has also been done to integrate macrophyte growth and decomposition with ecosystem processes and the broader biogeochemical cycles. On the other hand, the interplay between phytoplankton and macrophyte communities has received less attention and even less so the succession patterns and inter-specific competition within the macrophyte assemblage.

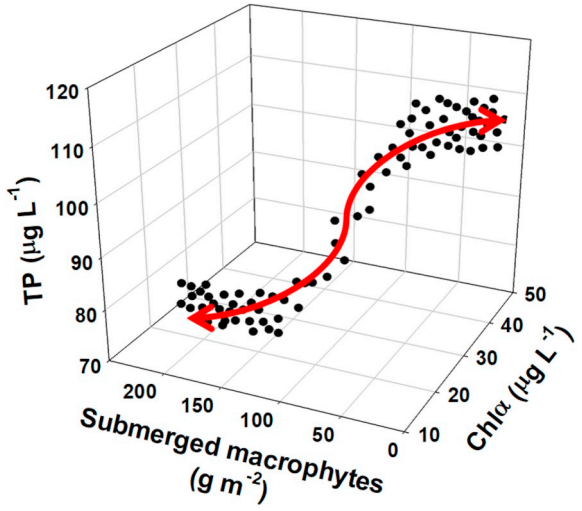

Fig. 4. *WEM*-predicted regime shift from a phytoplankton-dominated turbid state to a clear submerged macrophyte-dominated state. The non-linear shift of the seasonal (May–October) average values of TP ($\mu g\,L^{-1}$), chl*a* ($\mu g\,L^{-1}$), and macrophyte biomass ($g\,m^{-2}$) is the combined result of the variation in exogenous *P* loading (20.3–27.1 $kg\,day^{-1}$), respiration (0.0135–0.0165 day^{-1}) and mortality (0.0432–0.0528 day^{-1}) of submerged macrophytes, and *P* fraction in macrophyte biomass (0.0025–0.0125 g *P* g DW^{-1}).

- Using two sensitivity analysis methods (linear regression and Self-Organizing Maps), we evaluated the ability of our model to reproduce different aspects of wetland dynamics, including the potential of a non-linear shift from a turbid phytoplankton-dominated to a clear macrophyte-dominated state. Within the selected layout, i.e., induced perturbations reflecting the nutrient loading variability observed during the study period (1996–2012) and evaluation of model predictions after averaging over the growing season, our sensitivity analysis showed that the relationship between nutrient inflows and model outputs can be approximated as linear. It can thus be inferred that the system does not reach its carrying capacity, but there is also no evidence of an abrupt shift into a more favorable state within the typically prevailing external loading conditions. Our analysis shows that the external loading from Spencer and Chedoke creeks predominantly shape the ambient *TP* and Chl*a* dynamics, as well as the total macrophyte abundance in Cootes Paradise marsh. Effluent discharges from the Dundas *WWTP* and the *CSO*s accounted for nearly 20% of the total variability in the system. Given the recent *WWTP* upgrades to reduce nutrient effluents and eliminate the discharges from *CSO*s, our sensitivity exercise highlights the role of nutrient loading from the local tributaries as a critical factor for future wetland management.
- When ecological (biological rates, half saturation constants) and sediment parameters are considered, the residual variability of our linear sensitivity analysis can be up to 35%, and thus *SOM* analysis may be more suitable to capture complex non-linear patterns and to quantify the most influential model inputs. Consistent with earlier modelling work (Kim et al., 2016), our study identified the sedimentation of particulate matter and nutrient release from the sediments as two critical processes to characterize the phosphorus cycle in the wetland. In particular, several parameters that specify the fate and transport of phosphorus within the sediments, such as the sediment porosity affecting the degree of phosphorus dilution in the pore water, the sediment decomposition rate for refractory phosphorus, the dissolved phosphorus in the sediment pore water, as well as the diffusive reflux rate, appear to shape the magnitude of Fickian diffusive reflux from the sediments to the water column. In the same context, a critical question that could be extracted by *WEM* is the relative contribution of internal nutrient loading vis-à-vis the external inflows, as field and lab experiments corroborate recent modelling evidence that internal loading due to resuspension, mineralization, and reflux contribute close to 35% of the *TP* loading to Cootes Paradise (Kelton and Chow-Fraser, 2005; Mayer et al., 2005).
- Although the ambient *TP* levels remained fairly high ($> 130\,\mu g\,L^{-1}$), the present modelling exercise was able to reproduce alternative states of the algal-macrophyte competition (high phytoplankton-low macrophyte biomass and vice versa) within the domain of the model input space (parameter ranges and nutrient-loading variability) examined. Interestingly, our model provides evidence of a positive covariance among the submerged, emergent, and meadow macrophytes, in that either all three functional groups coexist with high abundance levels (Clusters 2, 4, and 5 in Table 4) or all are practically eliminated from the system (Clusters 1 and 3). The former scenario is suggestive of a synergistic effect through which a thriving meadow and emergent vegetation paves the way (stabilization of the sediments, increased competition with the algal assemblage) for submerged macrophytes to sustain themselves and effectively proliferate in the system. On the other hand, the latter pattern shows that once emergent and meadow macrophytes disappear, the submerged vegetation seemingly has a competitive handicap against phytoplankton, despite the capacity to uptake nutrients from two pathways (sediments and water column). According to our modelling analysis, the competitive advantage of phytoplankton stems from their ability to adapt in poorly illuminated environments, which is conceptually reinforced by the empirical evidence from Cootes Paradise of an algal assemblage typically dominated by cryptomonads, euglenophytes, and chlorophytes (Chow-Fraser et al., 1998). It is also worth noting that although the positive covariance among the residents of the macrophyte assemblage was predominantly triggered by the specification of water temperature control on emergent and meadow macrophyte growth in our simulations, other -more relevant to Cootes Paradise- factors that could conceivably induce the same structural shifts (i.e., render a resilient/susceptible emergent/meadow vegetation) are the water level fluctuations (Chow-Fraser, 2005) or the outcome of the ongoing planting efforts of emergent macrophytes (Theÿsmeÿer et al., 2016).
- Our model predicts that a drastic reduction of the external nutrient loading in Cootes Paradise could indeed induce an abrupt, non-linear shift from the current turbid-phytoplankton dominated state to its former clear-macrophyte dominated state. Nonetheless, we also found that the trajectory followed is also influenced by the assumptions made regarding the ability of macrophytes to sequester phosphorus. In particular, the specification of the internal phosphorus content plays a pivotal role not only in the amount of phosphorus taken up per unit of plant tissue formed, but also in determining the leachable P pool that can be returned into the water column through senescence or bacterial decomposition of decaying plant material (Granéli and Solander, 1988). In particular, emergent macrophytes usually possess large, perennial storage organs for carbohydrates and supporting tissues which are resistant to microbial attack, while submerged plants generally have only fine roots and do not contain much cellulose, and thus are more easily mineralized upon death (Twilley et al., 1986). The latter pattern is highly relevant to the current state of Cootes Paradise, when dominant species of the Pondweed family (e.g., *P. foliosus*) can spread in a fairly aggressive manner in the shallow, slow-moving waters of the marsh at the beginning of the growing season, but soon thereafter these submerged aquatic plants collapse and the decomposition of their dead tissues rapidly leads to a dramatic deterioration of the water quality conditions (Jennifer Bowman personal communication, April 24, 2018).

To recap, founded upon the reproduction of the resource competition among different phytoplankton and macrophyte functional groups,

WEM provides a means to explore ecological regime shifts between alternative stable states and offers new insights into wetland management. In an upcoming follow-up paper (Kim et al., 2018), we implement *WEM* to simulate the observed water quality dynamics in Cootes Paradise marsh and subsequently evaluate nutrient loading scenarios. This will allow us to evaluate the achievability (and associated uncertainty) of eutrophication targets in relation to how close we are to instigating a shift from the marsh's current turbid phytoplankton-dominated state to a desirable clear macrophyte-dominated state.

Acknowledgements

This project has received funding support from the Ontario Ministry of the Environment, Conservation and Parks (Canada-Ontario Grant Agreement 120808). Such support does not indicate endorsement by the Ministry of the contents of this material.

Appendix A. Supplementary data

Supplementary data to this article can be found online at https://doi.org/10.1016/j.ecoinf.2018.09.010.

References

Anderson, I.C., Tobias, C.R., Neikirk, B.B., Wetzel, R.L., 1997. Development of a process-based nitrogen mass balance model for a Virginia (USA) *Spartina alterniflora* salt marsh: implications for net DIN flux. Mar. Ecol. Prog. Ser. 159, 13–27. https://doi.org/10.3354/meps159013.

Arhonditsis, G.B., Brett, M.T., 2005. Eutrophication model for Lake Washington (USA) Part I. Model description and sensitivity analysis. Ecol. Model. 187, 140–178. https://doi.org/10.1016/j.ecolmodel.2005.01.040.

Asaeda, T., Karunaratne, S., 2000. Dynamic modeling of the growth of Phragmites australis: model description. Aquat. Bot. 67, 301–318. https://doi.org/10.1016/S0304-3770(00)00095-4.

Asaeda, T., Van Bon, T., 1997. Modelling the effects of macrophytes on algal blooming in eutrophic shallow lakes. Ecol. Model. 104, 261–287. https://doi.org/10.1016/S0304-3800(97)00129-4.

Asaeda, T., Trung, V.K., Manatunge, J., 2000. Modeling the effects of macrophyte growth and decomposition on the nutrient budget in Shallow Lakes. Aquat. Bot. 68, 217–237. https://doi.org/10.1016/S0304-3770(00)00123-6.

Asaeda, T., Trung, V.K., Manatunge, J., Van Bon, T., 2001. Modelling macrophyte–nutrient–phytoplankton interactions in shallow eutrophic lakes and the evaluation of environmental impacts. Ecol. Eng. 16, 341–357. https://doi.org/10.1016/S0925-8574(00)00120-8.

Barko, J.W., Smart, R.M., 1980. Mobilization of sediment phosphorus by submersed freshwater macrophytes. Freshw. Biol. 10, 229–238. https://doi.org/10.1111/j.1365-2427.1980.tb01198.x.

Blumer, A., Ehrenfeucht, A., Haussler, D., Warmuth, M.K., 1987. Occam's Razor. Inf. Process. Lett. 24, 377–380. https://doi.org/10.1016/0020-0190(87)90114-1.

Bolpagni, R., Bresciani, M., Laini, A., Pinardi, M., Matta, E., Ampe, E.M., Giardino, C., Viaroli, P., Bartoli, M., 2014. Remote sensing of phytoplankton-macrophyte coexistence in shallow hypereutrophic fluvial lakes. Hydrobiologia 737, 67–76. https://doi.org/10.1007/s10750-013-1800-6.

Carignan, R., Kalff, J., 1982. Phosphorus release by submerged macrophytes: significance to epiphyton and phytoplankton. Limnol. Oceanogr. 27, 419–427. https://doi.org/10.4319/lo.1982.27.3.0419.

Carpenter, S.R., 1981. Submersed vegetation: an internal factor in lake ecosystem succession. Am. Nat. 118, 372–383. https://doi.org/10.1086/283829.

Cerco, C., Cole, T., 1994. CE-QUAL-ICM Three-Dimensional Eutrophication Model. U.S. Army Engineer Waterways Experiment Station, Vicksburg, MS.

Chon, T.-S., 2011. Self-Organizing Maps applied to ecological sciences. Ecol. Inform. 6, 50–61. https://doi.org/10.1016/j.ecoinf.2010.11.002.

Chow-Fraser, P., 2005. Ecosystem response to changes in water level of Lake Ontario marshes: lessons from the restoration of Cootes Paradise Marsh. Hydrobiologia 539, 189–204. https://doi.org/10.1007/s10750-004-4868-1.

Chow-Fraser, P., Lougheed, V., Le Thiec, V., Crosbie, B., Simser, L., Lord, J., 1998. Long-term response of the biotic community to fluctuating water levels and changes in water quality in Cootes Paradise Marsh, a degraded coastal wetland of Lake Ontario. Wetl. Ecol. Manag. 6, 19–42. https://doi.org/10.1023/A:1008491520668.

Christiansen, N.H., Andersen, F.Ø., Jensen, H.S., 2016. Phosphate uptake kinetics for four species of submerged freshwater macrophytes measured by a 33P phosphate radioisotope technique. Aquat. Bot. 128, 58–67. https://doi.org/10.1016/j.aquabot.2015.10.002.

Chung, E.G., Bombardelli, F.A., Schladow, S.G., 2009. Modeling linkages between sediment resuspension and water quality in a shallow, eutrophic, wind-exposed lake. Ecol. Model. 220, 1251–1265. https://doi.org/10.1016/j.ecolmodel.2009.01.038.

Craft, C.B., 1997. Dynamics of nitrogen and phosphorus retention during wetland ecosystem succession. Wetl. Ecol. Manag. 4, 177–187. https://doi.org/10.1007/BF01879236.

Croft, M.V., Chow-Fraser, P., 2007. Use and development of the wetland macrophyte index to detect water quality impairment in fish habitat of Great Lakes coastal marshes. J. Great Lakes Res. 33, 172–197. https://doi.org/10.3394/0380-1330(2007)33[172:UADOTW]2.0.CO;2.

Cuddington, K., Fortin, M.J., Gerber, L.R., Hastings, A., Liebhold, A., O'Connor, M., Ray, C., 2013. Process-based models are required to manage ecological systems in a changing world. Ecosphere 4 (2), 1–12. https://doi.org/10.1890/ES12-00178.1.

Domin, A., Schubert, H., Krause, J.C., Schiewer, U., 2004. Modelling of pristine depth limits for macrophyte growth in the southern Baltic Sea. Hydrobiologia 514, 29–39. https://doi.org/10.1023/B:hydr.0000018204.47081.ae.

Dong, B.-C., Liu, R.-H., Yu, F.-H., 2015. Effects of *Spirogyra arcta* on biomass and structure of submerged macrophyte communities. Plant Spec. Biol. 30, 28–36. https://doi.org/10.1111/1442-1984.12036.

Environment Canada, 2006. Great Lakes Wetlands Conservation Action Plan Highlights Report 2003–2005. (Toronto, Ontario, Canada).

Falkowski, P.G., Owens, T.G., 1980. Light—shade adaptation: two strategies in marine phytoplankton. Plant Physiol. 66, 592–595. https://doi.org/10.1104/pp.66.4.592.

Frey, U.J., Rusch, H., 2013. Using artificial neural networks for the analysis of social-ecological systems. Ecol. Soc. 18 (2), 40. https://doi.org/10.5751/ES-05202-180240.

Giraudel, J.L., Lek, S., 2001. A comparison of self-organizing map algorithm and some conventional statistical methods for ecological community ordination. Ecol. Model. 146 (1–3), 329–339. https://doi.org/10.1016/S0304-3800(01)00324-6.

Granéli, W., Solander, D., 1988. Influence of aquatic macrophytes on phosphorus cycling in lakes. Hydrobiologia 170, 245–266. https://doi.org/10.1007/BF00024908.

Gudimov, A., Stremilov, S., Ramin, M., Arhonditsis, G.B., 2010. Eutrophication risk assessment in Hamilton Harbour: system analysis and evaluation of nutrient loading scenarios. J. Great Lakes Res. 36, 520–539. https://doi.org/10.1016/j.jglr.2010.04.001.

Gudimov, A., Kim, D.K., Young, J.D., Palmer, M.E., Dittrich, M., Winter, J.G., Stainsby, E., Arhonditsis, G.B., 2015. Examination of the role of dreissenids and macrophytes in the phosphorus dynamics of Lake Simcoe, Ontario, Canada. Ecol. Inform. 26, 36–53. https://doi.org/10.1016/j.ecoinf.2014.11.007.

Herb, W.R., Stefan, H.G., 2003. Integral growth of submersed macrophytes in varying light regimes. Ecol. Model. 168, 77–100. https://doi.org/10.1016/S0304-3800(03)00206-0.

Herb, W.R., Stefan, H.G., 2006. Seasonal growth of submersed macrophytes in lakes: the effects of biomass density and light competition. Ecol. Model. 193, 560–574. https://doi.org/10.1016/j.ecolmodel.2005.08.027.

Ikusima, I., 1970. Ecological studies on the productivity of aquatic plant communities IV: light condition and community photosynthesic production. Bot. Mag. Tokyo 83, 330–341. https://doi.org/10.15281/jplantres1887.83.330.

Janse, J.H., Scheffer, M., Lijklema, L., Van Liere, L., Sloot, J.S., Mooij, W.M., 2010. Estimating the critical phosphorus loading of shallow lakes with the ecosystem model PCLake: sensitivity, calibration and uncertainty. Ecol. Model. 221 (4), 654–665. https://doi.org/10.1016/j.ecolmodel.2009.07.023.

Julian, J.P., Seegert, S.Z., Powers, S.M., Stanley, E.H., Doyle, M.W., 2011. Light as a first-order control on ecosystem structure in a temperate stream. Ecohydrology 4 (3), 422–432. https://doi.org/10.1002/eco.144.

Kéfi, S., Holmgren, M., Scheffer, M., Pugnaire, F., 2015. When can positive interactions cause alternative stable states in ecosystems? Funct. Ecol. 30, 88–97. https://doi.org/10.1111/1365-2435.12601.

Keizer-Vlek, H.E., Verdonschot, P.F.M., Verdonschot, R.C.M., Dekkers, D., 2014. The contribution of plant uptake to nutrient removal by floating treatment wetlands. Ecol. Eng. 73, 684–690. https://doi.org/10.1016/j.ecoleng.2014.09.081.

Kelton, N., Chow-Fraser, P., 2005. A simplified assessment of factors controlling phosphorus loading from oxygenated sediments in a very shallow eutrophic lake. Lake Reserv. Manag. 21 (3), 223–230. https://doi.org/10.1080/07438140509354432.

Kim, D.-K., Zhang, W., Rao, Y.R., Watson, S., Mugalingam, S., Labencki, T., Dittrich, M., Morley, A., Arhonditsis, G.B., 2013. Improving the representation of internal nutrient recycling with phosphorus mass balance models: a case study in the Bay of Quinte, Ontario, Canada. Ecol. Model. 256, 53–68. https://doi.org/10.1016/j.ecolmodel.2013.02.017.

Kim, D.-K., Peller, T., Gozum, Z., Theÿsmeÿer, T., Long, T., Boyd, D., Watson, S., Rao, Y.R., Arhonditsis, G.B., 2016. Modelling phosphorus dynamics in Cootes Paradise Marsh: uncertainty assessment and implications for eutrophication management. Aquat. Ecosyst. Health Manag. 19, 368–381. https://doi.org/10.1080/14634988.2016.1255097.

Kim, D.K., Kaluskar, S., Mugalingam, S., Blukacz-Richards, A., Long, T., Morley, A., Arhonditsis, G.B., 2017. A Bayesian approach for estimating phosphorus export and delivery rates with the SPAtially Referenced Regression On Watershed attributes (SPARROW) model. Ecol. Inform. 37, 77–91. https://doi.org/10.1016/j.ecoinf.2016.12.003.

Kim D.K.,Yang, C., Javed, A., Parsons, C.T., Bowman, J.E., Theÿsmeÿer, T., Arhonditsis, G.B., 2018. Evaluating the uncertainty with the management of a eutrophic wetland: how useful are the process-based models? (Submitted Manuscript).

Köhler, J., Hachoł, J., Hilt, S., 2010. Regulation of submersed macrophyte biomass in a temperate lowland river: interactions between shading by bank vegetation, epiphyton and water turbidity. Aquat. Bot. 92, 129–136. https://doi.org/10.1016/j.aquabot.2009.10.018.

Kohonen, T., 1997. Self-Organizing Maps. Springer, New York (426 pp.).

Kohonen, T., 2001. Self-Organizing Maps, 3rd ed. Springer, New York.

Korboulewsky, N., Wang, R., Baldy, V., 2012. Purification processes involved in sludge treatment by a vertical flow wetland system: focus on the role of the substrate and plants on N and P removal. Bioresour. Technol. 105, 9–14. https://doi.org/10.1016/j.biortech.2011.11.037.

Kurtz, J.C., Yates, D.F., Macauley, J.M., Quarles, R.L., Genthner, F.J., Chancy, C.A., Devereux, R., 2003. Effects of light reduction on growth of the submerged macrophyte Vallisneria americana and the community of root-associated heterotrophic bacteria. J. Exp. Mar. Biol. Ecol. 291, 199–218. https://doi.org/10.1016/S0022-0981(03)00120-5.

Kuusemets, V., Lohmus, K., 2005. Nitrogen and phosphorus accumulation and biomass production by Scirpus sylvaticus and Phragmites australis in a horizontal subsurface flow constructed wetland. J. Environ. Sci. Health A 40 (6–7), 1167–1175. https://doi.org/10.1081/ESE-200055629.

Leisti, K.E., Theÿsmeÿer, T., Doka, S.E., Court, A., 2016. Aquatic vegetation trends from 1992 to 2012 in Hamilton Harbour and Cootes Paradise, Lake Ontario. Aquat. Ecosyst. Health Manag. 19, 219–229. https://doi.org/10.1080/14634988.2015.1129257.

Li, J., Huang, P., Zhang, R., 2010. Modeling the refuge effect of submerged macrophytes in ecological dynamics of shallow lakes: a new model of fish functional response. Ecol. Model. 221, 2076–2085. https://doi.org/10.1016/j.ecolmodel.2010.05.005.

Li, X., Cui, B., Yang, Q., Lan, Y., Wang, T., Han, Z., 2013. Effects of plant species on macrophyte decomposition under three nutrient conditions in a eutrophic shallow lake, North China. Ecol. Model. 252, 121–128. https://doi.org/10.1016/j.ecolmodel.2012.08.006.

Li, J., Yang, X., Wang, Z., Shan, Y., Zheng, Z., 2015. Comparison of four aquatic plant treatment systems for nutrient removal from eutrophied water. Bioresour. Technol. 179, 1–7. https://doi.org/10.1016/j.biortech.2014.11.053.

Lougheed, V.L., Crosbie, B., Chow-Fraser, P., 1998. Predictions on the effect of common carp (*Cyprinus carpio*) exclusion on water quality, zooplankton, and submergent macrophytes in a Great Lakes wetland. Can. J. Fish. Aquat. Sci. 55, 1189–1197. https://doi.org/10.1139/f97-315.

Lougheed, V.L., Theÿsmeÿer, T., Smith, T., Chow-Fraser, P., 2004. Carp exclusion, food-web interactions, and the restoration of Cootes Paradise marsh. J. Great Lakes Res. 30, 44–57. https://doi.org/10.1016/S0380-1330(04)70328-7.

Lundholm, J.T., Simser, W.L., 1999. Regeneration of submerged macrophyte populations in a disturbed Lake Ontario coastal marsh. J. Great Lakes Res. 25 (2), 395–400.

Lv, D., Fan, M., Kang, Y., Blanco, K., 2016. Modeling refuge effect of submerged macrophytes in lake system. B. Math. Biol. 78, 662–694. https://doi.org/10.1007/s11538-016-0154-4.

Mayer, T., Rosa, F., Charlton, M., 2005. Effect of sediment geochemistry on the nutrient release rates in Cootes Paradise Marsh, Ontario, Canada. Aquat. Ecosyst. Health Manag. 8, 133–145. https://doi.org/10.1080/14634980590954986.

McNair, S.A., Chow-Fraser, P., 2003. Change in biomass of benthic and planktonic algae along a disturbance gradient for 24 Great Lakes coastal wetlands. C. J. F. Aquat. Sci. 60 (6), 676–689. https://doi.org/10.1139/f03-054.

Mehta, A.J., Parchure, T.M., Dixit, J.G., Ariathurai, R., 1982. Resuspension potential of deposited cohesive sediment beds. In: Kennedy, V.S. (Ed.), Estuarine Comparisons. Academic Press, New York, pp. 591–609. https://doi.org/10.1016/B978-0-12-404070-0.50042-9.

Miller, J.K., Roketenetz, L., Garris, H., 2011. Modeling the interaction between the exotic invasive aquatic macrophyte Myriophyllum spicatum and the native biocontrol agent Euhrychiopsis lecontei to improve augmented management programs. BioControl 56, 935–945. https://doi.org/10.1007/s10526-011-9371-9.

Minns, C.K., 1986. A simple whole-lake phosphorus model and a trial application to the Bay of Quinte. In: Minns, C.K., Hurley, D.A., Nicholls, K.H. (Eds.), Project Quinte: Point-Source Phosphorus Control and Ecosystem Response in the Bay of Quinte, Lake Ontario. Canadian Special Publication of Fisheries and Aquatic Sciences, Ottawa, ON, Canada, pp. 84–90.

Moore, R.B., Johnson, C.M., Robinson, K.W., Deacon, J.R., 2004. Estimation of Total Nitrogen and Phosphorus in New England Streams Using Spatially Referenced Regression Models. US Department of the Interior, US Geological Survey, New Hampshire.

Mulder, C., Hendriks, A.J., 2014. Half-saturation constants in functional responses. Glob. Ecol. Conserv. 2, 161–169. https://doi.org/10.1016/j.gecco.2014.09.006.

Mulderij, G., Van Nes, E.H., Van Donk, E., 2007. Macrophyte–phytoplankton interactions: the relative importance of allelopathy versus other factors. Ecol. Model. 204, 85–92. https://doi.org/10.1016/j.ecolmodel.2006.12.020.

Park, S.S., Uchrin, C.G., 1997. A stoichiometric model for water quality interactions in macrophyte dominated water bodies. Ecol. Model. 96, 165–174. https://doi.org/10.1016/S0304-3800(96)00064-6.

Park, Y.S., Kwon, Y.S., Hwang, S.J., Park, S., 2014. Characterizing effects of landscape and morphometric factors on water quality of reservoirs using a self-organizing map. Environ. Model Softw. 55, 214–221. https://doi.org/10.1016/j.envsoft.2014.01.031.

Paudel, R., Jawitz, J.W., 2012. Does increased model complexity improve description of phosphorus dynamics in a large treatment wetland? Ecol. Eng. 42, 283–294. https://doi.org/10.1016/j.ecoleng.2012.02.014.

Pelton, D.K., Levine, S.N., Braner, M., 1998. Measurements of phosphorus uptake by macrophytes and epiphytes from the LaPlatte River (VT) using 32P in stream microcosms. Freshw. Biol. 39 (2), 285–299. https://doi.org/10.1046/j.1365-2427.1998.00281.x.

Plus, M., Chapelle, A., Lazure, P., Auby, I., Levavasseur, G., Verlaque, M., Belsher, T., Deslous-Paoli, J.-M., Zaldivar, J., Murray, C., 2003. Modelling of oxygen and nitrogen cycling as a function of macrophyte community in the Thau lagoon. Cont. Shelf Res. 23, 1877–1898. https://doi.org/10.1016/j.csr.2003.03.001.

Raeder, U., Ruzicka, J., Goos, C., 2010. Characterization of the light attenuation by periphyton in lakes of different trophic state. Limnologica 40, 40–46. https://doi.org/10.1016/J.LIMNO.2009.01.001.

Ramin, M., Stremilov, S., Labencki, T., Gudimov, A., Boyd, D., Arhonditsis, G.B., 2011. Integration of numerical modeling and Bayesian analysis for setting water quality criteria in Hamilton Harbour, Ontario, Canada. Environ. Model Softw. 26, 337–353. https://doi.org/10.1016/j.envsoft.2010.08.006.

Routledge, I., 2012. City of Hamilton Wastewater Treatment Facitlities 2011 Annual Report: CSO Tanks report (Hamilton, Ontario, Canada). 2012.

Sand-Jensen, K., Borum, J., 1984. Epiphyte shading and its effect on photosynthesis and diel metabolism of Lobelia dortmanna L. during the spring bloom in a Danish lake. Aquat. Bot. 20 (1–2), 109–119. https://doi.org/10.1016/0304-3770(84)90031-7.

Schallenberg, M., Sorrell, B., 2009. Regime shifts between clear and turbid water in New Zealand lakes: environmental correlates and implications for management and restoration. N. Z. J. Mar. Freshw. Res. 43, 701–712.

Scheffer, 1990. Multiplicity of stable states in freshwater systems. Hydrobiologia 200/201, 475–486. https://doi.org/10.1007/BF02530365.

Scheffer, M., Rinaldi, S., Gragnani, A., Mur, L.R., van Nes, E.H., 1997. On the dominance of filamentous cyanobacteria in shallow, turbid lakes. Ecology 78 (1), 272–282. https://doi.org/10.1890/0012-9658(1997)078[0272:OTDOFC]2.0.CO;2.

Scheffer, M., Carpenter, S., Foley, J.A., Folke, C., Walker, B., 2001. Catastrophic shifts in ecosystems. Nature 413, 591–596. https://doi.org/10.1038/35098000.

Short, F.T., McRoy, C.P., 1984. Nitrogen uptake by leaves and roots of the seagrass Zostera marina L. Bot. Mar. 27 (12), 547–556. https://doi.org/10.1515/botm.1984.27.12.547.

Smith, P.G.R., Glooschenko, V., Hagen, D.A., 1991. Coastal wetlands of three Canadian Great Lakes: inventory, current conservation initiatives, and patterns of variation. Can. J. Fish. Aquat. Sci. 48, 1581–1594. https://doi.org/10.1139/f91-187.

Soldat, D.J., Petrovic, A.M., 2008. The fate and transport of phosphorus in turfgrass ecosystems. Crop Sci. 48, 2051–2065. https://doi.org/10.2135/cropsci2008.03.0134.

Suding, K.N., Gross, K.L., Houseman, G.R., 2004. Alternative states and positive feedbacks in restoration ecology. Trends Ecol. Evol. 19, 46–53. https://doi.org/10.1016/j.tree.2003.10.005.

Tabou, T.T., Baya, D.T., Eyul'anki, D.M., Vasel, J.L., 2014. Monitoring the influence of light intensity on the growth and mortality of duckweed (Lemna minor) through digital images processing. In: 10th IWA Specialist Group Conference on Ponds Technology: Advances and Innovations in Pond Treatment Technology, (Cartagena, Colombie).

Tanner, C.C., Headley, T.R., 2011. Components of floating emergent macrophyte treatment wetlands influencing removal of stormwater pollutants. Ecol. Eng. 37 (3), 474–486. https://doi.org/10.1016/j.ecoleng.2010.12.012.

Theÿsmeÿer, T., 2011. Project Paradise Planning to 2015: RBG Contribution to the HHRAP for the Restoration of the Wetlands. Natural Lands Deparment, Royal Botanical Gardens (RBG), Burlington, ON, Canada.

Theÿsmeÿer, T., Bowman, J., 2017. Western Desjardins Canal and West Pond Conditions Summary Report. Internal Report No. 2017–1. (Hamilton, ON, Canada).

Theÿsmeÿer, T., Reich, B., Bowman, J.E., 2009. Water Quality Characterization of the Main Tributaries of the Garden's Property – Spencer Creek, Chedoke Creek, Borer's Creek and Grindstone Creek. Royal Botanical Gardens, Burlington, ON, Canada.

Theÿsmeÿer, T., Bowman, J., Court, A., Richer, S., 2016. Wetlands Conservation Plan 2016–2021. Natural Lands Department. Internal Report No. 2016–1. Royal Botanical Gardens, Hamilton, Ontario, Canada.

Thomasen, S., Chow-Fraser, P., 2012. Detecting changes in ecosystem quality following long-term restoration efforts in Cootes Paradise Marsh. Ecol. Indic. 13, 82–92. https://doi.org/10.1016/j.ecolind.2011.04.036.

Tobias, C.R., Anderson, I.C., Canuel, E.A., Macko, S.A., 2001. Nitrogen cycling through a fringing marsh-aquifer ecotone. Mar. Ecol. Prog. Ser. 210, 25–39. https://doi.org/10.3354/meps210025.

Twilley, R.R., Ejdung, G., Romare, P., Kemp, W.M., 1986. A comparative study of decomposition, oxygen consumption and nutrient release for selected aquatic plants occurring in an estuarine environment. Oikos 47, 190–198. https://doi.org/10.2307/3566045.

Verhoeven, J.T.A., Arheimer, B., Yin, C., Hefting, M.M., 2006. Regional and global concerns over wetlands and water quality. Trends Ecol. Evol. 21, 96–103. https://doi.org/10.1016/j.tree.2005.11.015.

Vesanto, J., Alhoniemi, E., 2000. Clustering of the Self-Organizing Map. IEEE Trans. Neural Netw. 11, 586–600. https://doi.org/10.1109/72.846731.

Vesanto, J., Himberg, J., Alhoniemi, E., Parhankangas, J., 2000. SOM Toolbox for Matlab 5. Helsinki University of Technology, Finland.

Wade, A.J., Hornberger, G.M., Whitehead, P.G., Jarvie, H.P., Flynn, N., 2001. On modeling the mechanisms that control in-stream phosphorus, macrophyte, and epiphyte dynamics: an assessment of a new model using general sensitivity analysis. Water Resour. Res. 37, 2777–2792. https://doi.org/10.1029/2000WR000115.

Wade, A.J., Whitehead, P.G., Hornberger, G.M., Jarvie, H.P., Flynn, N., 2002a. On modelling the impacts of phosphorus stripping at sewage works on in-stream phosphorus and macrophyte/epiphyte dynamics: a case study for the River Kennet. Sci. Total Environ. 282–283, 395–415. https://doi.org/10.1016/S0048-9697(01)00926-3.

Wade, A.J., Whitehead, P.G., Hornberger, G.M., Snook, D.L., 2002b. On modelling the flow controls on macrophyte and epiphyte dynamics in a lowland permeable catchment: the River Kennet, southern England. Sci. Total Environ. 282–283, 375–393. https://doi.org/10.1016/S0048-9697(01)00925-1.

Wang, J., 2014. Combined sewer overflows (CSOs) impact on water quality and environmental ecosystem in the Harlem River. Earth Environ. Sci. 5 (13), 1373–1389. https://doi.org/10.4236/jep.2014.513131.

Wang, C.Y., Sample, D.J., Day, S.D., Grizzard, T.J., 2015. Floating treatment wetland nutrient removal through vegetation harvest and observations from a field study. Ecol. Eng. 78, 15–26. https://doi.org/10.1016/j.ecoleng.2014.05.018.

Wellen, C., Arhonditsis, G.B., Labencki, T., Boyd, D., 2014a. Application of the SPARROW model in watersheds with limited information: a Bayesian assessment of the model uncertainty and the value of additional monitoring. Hydrol. Process. 28, 1260–1283.

https://doi.org/10.1002/hyp.9614.
Wellen, C., Arhonditsis, G.B., Long, T., Boyd, D., 2014b. Quantifying the uncertainty of nonpoint source attribution in distributed water quality models: a Bayesian assessment of SWAT's sediment export predictions. J. Hydrol. 519, 3353–3368. https://doi.org/10.1016/j.jhydrol.2014.10.007.
Winter, J.G., Duthie, H.C., 2000. Export coefficient modeling to assess phosphorus loading in an urban watershed. J. Am. Water Resour. Assoc. 36, 1053–1061. https://doi.org/10.1111/j.1752-1688.2000.tb05709.x.
Wroblewski, J.S., 1980. A simulation of the distribution of Acartia clausi during Oregon upwelling, August 1973. J. Plankton Res. 2 (1), 43–68. https://doi.org/10.1093/plankt/2.1.43.
Xu, F.L., Jørgensen, S.E., Tao, S., 1999. Ecological indicators for assessing freshwater ecosystem health. Ecol. Model. 116 (1), 77–106. https://doi.org/10.1016/S0304-3800(98)00160-4.
Zhang, J., Jørgensen, S.E., Beklioglu, M., Ince, O., 2003. Hysteresis in vegetation shift—Lake Mogan prognoses. Ecol. Model. 164 (2–3), 227–238. https://doi.org/10.1016/S0304-3800(03)00050-4.
Zimmerman, R.C., Pasini, A.C., Alberte, R.S., 1994. Modeling daily production of aquatic macrophytes from irradiance measurements: a comparative analysis. Mar. Ecol. Prog. Ser. 114 (1–2), 185–196. https://doi.org/10.3354/meps114185.

DEVELOPMENT OF A MECHANISTIC EUTROPHICATION MODEL FOR WETLAND MANAGEMENT: SENSITIVITY ANALYSIS OF THE INTERPLAY AMONG PHYTOPLANKTON, MACROPHYTES, AND SEDIMENT NUTRIENT RELEASE

[SUPPORTING INFORMATION]

Dong-Kyun Kim, Aisha Javed, Cindy Yang, George B. Arhonditsis*

Ecological Modelling Laboratory

Department of Physical & Environmental Sciences, University of Toronto,

Toronto, Ontario, Canada, M1C1A4

* Corresponding author

Email: georgea@utsc.utoronto.ca, Tel.: +1 416 208 4858; Fax: +1 416 287 7279

Figure S1: Self Organizing Map outputs consisting of four (4) external forcing functions, fourteen (14) model parameters, ten (10) state variables, and twelve (12) *TP*-flux values. Symbols are provided in Table S2.

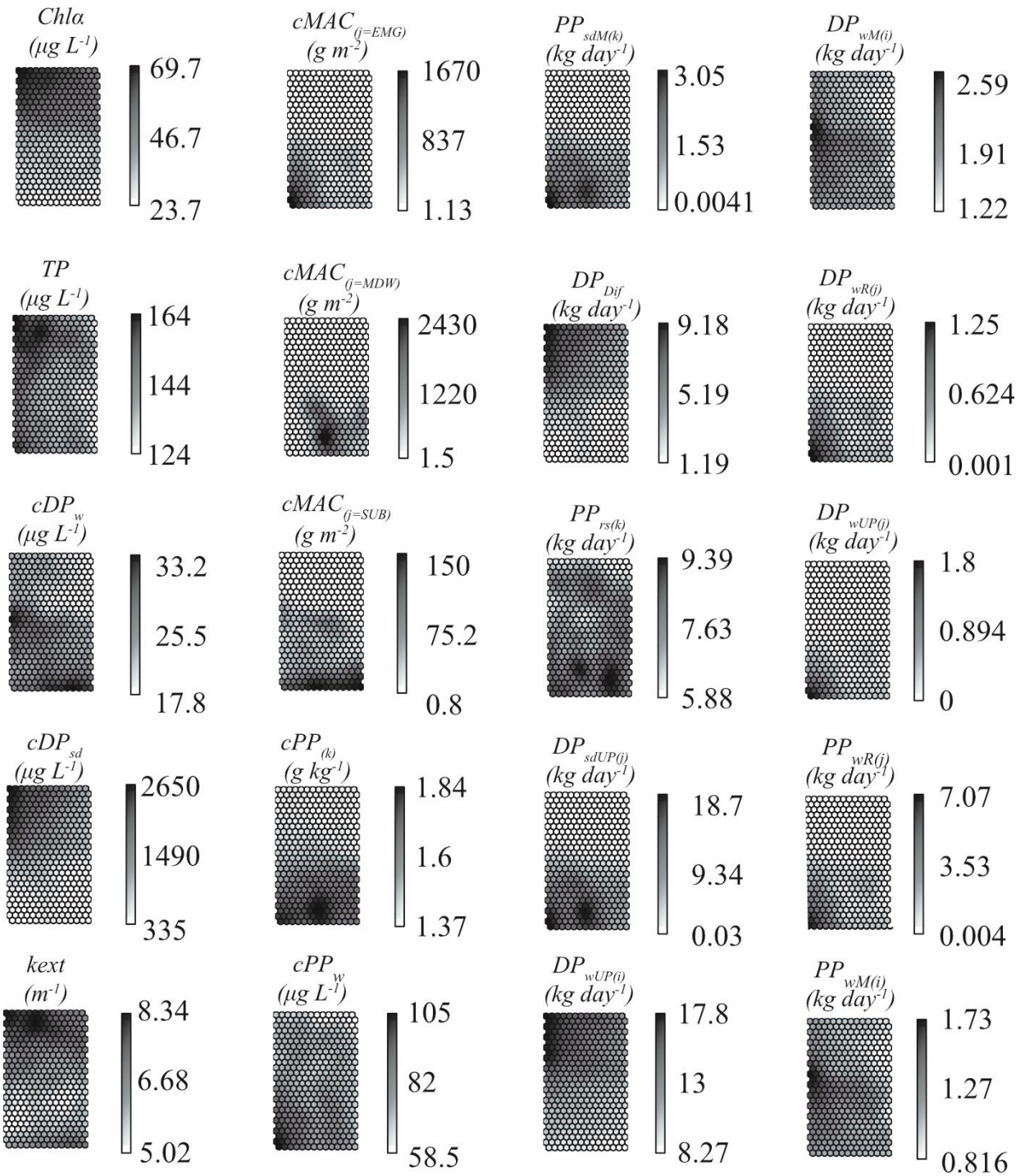

Figure S1: (Continued)

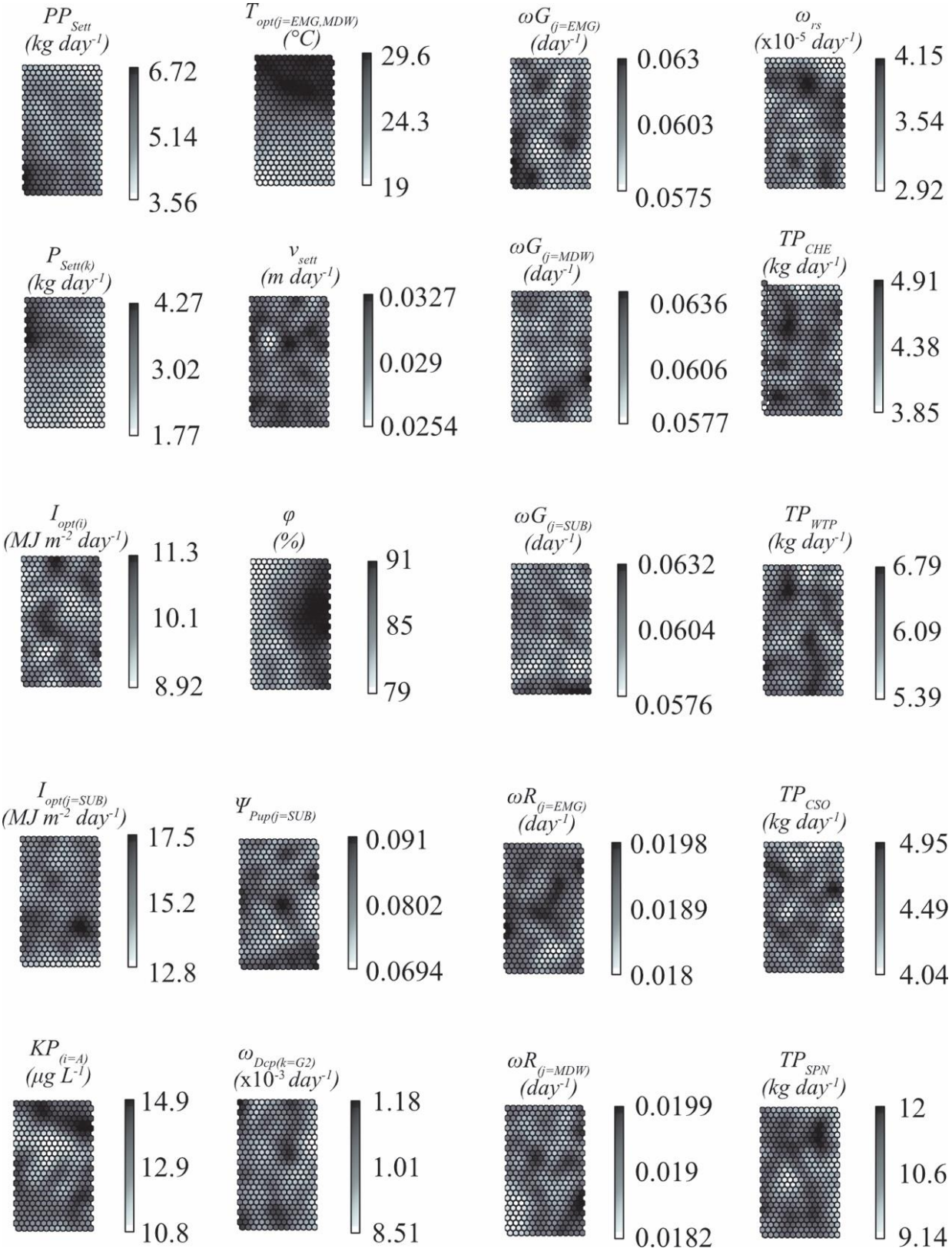

Table S1: Wetland Eutrophication Model (*WEM*) mathematical equations, where *i* = phytoplankton *A, B*, and *C*; *j* = macrophytes meadow (*MDW*), emergent (*EMG*), and submerged (*SUB*); and *k* = *G1* (labile), *G2* (refractory), and *G3* (inert).

Process	*Symbol*	*Equation*
Dissolved Phosphorous in Water Column	DP_w	$DP_{wIN} + DP_{wM(i)} + PP_{MN} + DP_{Dif} + DP_{wR(j)} - DP_{wOUT} - DP_{wUP(i)} - DP_{wUP(j)}$
	DP_{wIN}	$DP_{wBack} + DP_{wEXT}$
	DP_{wBack}	$BF_{HH} \cdot \Psi_{HH} \cdot cTP_{Back} \cdot 10^{-6}$
	DP_{Dif}	$\omega_{Dif} \cdot \alpha_{Rst} \cdot (cDP_w - cDP_{sd}) \cdot V_{sd} \cdot \theta_{Dif}^{(T_{sd}-T_{Ref})} \cdot 10^{-6}$
	T_{sd}	$8.6 \cdot sin\left(\frac{2\pi t}{365} - 2.136\right) + 11$
	$DP_{wM(i)}$	$\sum \Psi_{mP_{(i)}} \cdot D_{(i)} \cdot P_{(i)} \cdot cPHYT_{(i)} \cdot V \cdot 10^{-6}$
	$D_{(i)}$	$\omega_{M_{(i)}} \cdot e^{\theta_{M(i)}(T-T_{Ref})}$
	$\frac{\partial P_{(i)}}{\partial t}$	$P_{up(i)} - \omega_{G_{(i)}} \cdot P_{(i)}$
	$P_{up(i)}$	$\omega_{maxUP(i)} \cdot \frac{cDP_w}{cDP_w + KP_{(i)}} \cdot \left(\frac{P_{max(i)} - P_{(i)}}{P_{max(i)} - P_{min(i)}}\right)$
	PP_{MN}	$KP_{MN} \cdot cPP_w \cdot V \cdot 10^{-6}$
	KP_{MN}	$\omega_{MN} \cdot e^{-\theta_{MN} \cdot (T-T_{Ref})^2}$
	$DP_{wR(j)}$	$\sum \left(\omega_{R_{(j)}} \cdot cMAC_{(j)} \cdot \mu_{P/DW} \cdot A_{(j)} \cdot \Psi_{R_{(j)}}\right) \cdot \alpha_{Rst} \cdot \Psi_{MET(j)} \cdot 10^{-3}$
	α_{Rst}	$1 - \left(\epsilon_{\alpha(j)} \cdot \frac{cMAC_{(j=SUB)}}{cMAC_{AVE} + cMAC_{(j=SUB)}}\right)$

	DP_{wOUT}	$cDP_w \cdot \omega_{HH_{OUT}} \cdot 10^{-6}$
	$DP_{wUP(i)}$	$\sum P_{up(i)} \cdot cPHYT_{(i)} \cdot V \cdot 10^{-6}$
	$DP_{wUP(j)}$	$\sum G_{(j)} \cdot A_{(j)} \cdot cMAC_{(j)} \cdot \mu_{P/DW} \cdot \left(1 - \Psi_{Pup(j)}\right) \cdot 10^{-3}$
	$\Psi_{Pup(j)}$	$\frac{cDP_{sd}/KP_{sd(j)} \cdot \Psi_{Nut(j)}}{\left(cDP_{sd}/KP_{sd(j)} \cdot \Psi_{Nut(j)}\right) + \left(cDP_w/KP_{w(j)} \cdot \left(2 - \Psi_{Nut(j)}\right)\right)}$
Particulate Phosphorous in the Water Column	PP_w	$PP_{wIN} + PP_{wM(i)} + PP_{wR(j)} + PP_{rs(k)} - PP_{Sett} - PP_{MN} - PP_{OUT}$
	PP_{wIN}	$\left(1 - \frac{DP_{wIN}}{TP_{IN}}\right) \cdot TP_{IN}$
	$PP_{wM(i)}$	$\sum \left(1 - \Psi_{mP_{(i)}}\right) \cdot D_{(i)} \cdot P_{(i)} \cdot cPHYT_{(i)} \cdot \frac{V}{10^6}$
	$PP_{wR(j)}$	$\sum \omega_{R(j)} \cdot cMAC_{(j)} \cdot \mu_{P/DW} \cdot A_{(j)} \cdot \left(1 - \Psi_{R_{(j)}}\right) \cdot \alpha_{Rst} \cdot 10^{-3}$
	$PP_{rs(k)}$	$\frac{R_{rs} \cdot A_{acc} \cdot \alpha_{Rst} \cdot \Psi_{rs_{(k)}}}{10^6}$
	A_{acc}	$A \cdot \left(1 - \frac{Sd_{ACE}}{100}\right)$
	R_{rs}	$\begin{cases} \tau \geq \tau_c, & \epsilon_{rs} \cdot \left(\frac{\tau - \tau_c}{\tau_c}\right) \\ \tau < \tau_c, & 0 \end{cases}$
	ϵ_{rs}	$SSD \cdot H \cdot \left(1 - \frac{\sum A_{(j)}}{A}\right) \cdot \omega_{rs} \cdot 10^7$

	PP_{Sett}	$\frac{v_{sett} \cdot cPP_w \cdot V}{z} \cdot 10^{-6}$
	PP_{OUT}	$\omega_{HH_{OUT}} \cdot cPP_w \cdot 10^{-6}$
Phytoplankton in the Water Column	$\frac{\partial PHYT_{(i)}}{\partial t}$	$\left(G_{(i)} - D_{(i)} - \frac{v_{(i)}}{z} - \frac{\omega_{HH_{OUT}}}{V}\right) \cdot PHYT_{(i)} + PHYT_{Back(i)}$
	$G_{(i)}$	$\omega_{G_{(i)}} \cdot f_i(N) \cdot f_i(L) \cdot f_i(T)$
	$f_i(N)$	$\frac{P_{(i)} - P_{min(i)}}{P_{max(i)} - P_{min(i)}}$
	$f_i(L)$	$2.718 \cdot \left(\frac{FD}{kext \cdot z}\right)(e^{-x1} - e^{-x2})$
	$kext$	$kext_{\epsilon} + \sum\left(kext_{Chl\alpha(i)} \cdot \mu_{Chl\alpha/C} \cdot cPHYT_{(i)}\right) + kext_{SUB} \cdot cMAC_{(j=SUB)}{}^2$
	$x1$	$\frac{I_o e^{-kext \cdot z} \cdot f_{shade}}{FD \cdot I_{opt(i)}}$
	$x2$	$\frac{I_o \cdot f_{shade}}{FD \cdot I_{opt(i)}}$
	f_{shade}	$1 - \Psi_{S_a} \cdot \Psi_{max(j)} \cdot \left(\frac{cMAC_{(j=EMG)} + cMAC_{(j=MDW)}}{cMAC_{(j=EMG)} + cMAC_{(j=MDW)} + cMAC_{AVE}}\right)$
	$f_i(T)$	$e^{-\theta_{(i)}(T - T_{opt(i)})^2}$
	$PHYT_{Back(i)}$	$BF_{HH} \cdot cPHYT_{Back(i)} \cdot 10^{-6}$
Macrophytes	$\frac{\partial MAC_j}{\partial t}$	$A_{(j)} \cdot cMAC_{(j)}\left(G_{(j)} - R_{(j)} - D_{(j)}\right)$

	$G_{(j)}$	$\omega_{G(j)} \cdot f_j(L) \cdot f_j(N) \cdot f_j(T)$
	$f_{(j=EMG,MDW)}(L)$	$\frac{I_o}{I_{opt(j=EMG,MDW)}}$
	$f_{(j=SUB)}(L)$	$2.718 \cdot \left(\frac{FD}{kext \cdot z_{SUB}}\right) \cdot (e^{-x1} - e^{-x2})$
	$x1$	$\frac{I_o e^{-kext \cdot z} \cdot f_{shade}}{FD \cdot I_{opt(j=SUB)}}$
	$x2$	$\frac{I_o \cdot f_{shade}}{FD \cdot I_{opt(j=SUB)}}$
	$f_j(N)$	$\left(\frac{\Psi_{Pup(j)} \cdot cDP_{sd}}{KP_{sd(j)} + cDP_{sd}}\right) + \left(\frac{(1 - \Psi_{Pup(j)}) \cdot cDP_w}{KP_{w(j)} + cDP_w}\right)$
	$f_j(T)$	$\begin{cases} T \le T_{opt_{(j)}}, & e^{-\theta_{\epsilon 1} \cdot \left(T - T_{opt_{(j)}}\right)^2} \\ T > T_{opt_{(j)}}, & e^{-\theta_{\epsilon 2} \cdot \left(T - T_{opt_{(j)}}\right)^2} \end{cases}$
	$R_{(j)}$	$\omega_{R_{(j)}} \cdot \theta_{R(j)}^{(T - T_{Ref})^2}$
	$D_{(j)}$	$\omega_{D_{(j)}} \cdot \theta_{D(j)}^{(T - T_{Ref})^2}$
Dissolved Phosphorous in Interstitial Waters	DP_{Sd}	$PP_{Dcp(k)} - DP_{Dif} - DP_{SdUP(j)}$
	$PP_{Dcp(k)}$	$\sum \omega_{Dcp(k)} \cdot cPP_{(k)} \cdot \theta_{(k)}^{(T_{sd} - T_{Ref})^2} \cdot \frac{m_{sd}}{1000}$
	DP_{Dif}	$\omega_{Dif} \cdot (cDP_w - cDP_{Sd}) \cdot V_{sd} \cdot \theta_{Dif}^{(T_{Sd} - T_{Ref})^2} \cdot 10^{-6}$
	$DP_{SdUP(j)}$	$\sum G_{(j)} \cdot A_{(j)} \cdot cMAC_{(j)} \cdot \mu_{P/DW} \cdot 10^{-3} \cdot \Psi_{Pup(j)}$

Particulate Phosphorous in Sediment	$PP_{(k)}$	$\sum\left(PP_{IN(k)} - PP_{Dcp(k)} - PP_{rs(k)} - PP_{Br(k)}\right)$
	$PP_{IN(k)}$	$P_{Sett(k)} + PP_{sdM(k)} + PP_{Sett(k)}$
	$P_{Sett(k)}$	$\sum_{k}\sum_{i} PHYT_{(i)} \cdot \frac{v_{(i)}}{z} \cdot P_{(i)} \cdot \Psi_{PP(i,k)}$
	$PP_{sdM(k)}$	$\sum_{k}\sum_{j} \Psi_{PP(j,k)} \cdot MAC_{(j)} \cdot \mu_{P/DW} \cdot D_{(j)} \cdot 10^{-3} \cdot \Psi_{RET}$
	$PP_{Sett(k)}$	$\sum \Psi_{PP(k)} \cdot v_{sett} \cdot \left(1 - \frac{\sum cPP_{wM(i)}}{cPP_w}\right) \cdot cPP_w \cdot A \cdot 10^{-6}$
	$PP_{Br(k)}$	$\epsilon_{DepBr} \cdot cPP_{(k)} \cdot m_{sd} \cdot 10^{-3}$
	ϵ_{DepBr}	$\frac{cTSS \cdot v_{sett}}{Sd_{fact}} \cdot 10^{-7}$
	Sd_{fact}	$H \cdot SSD \cdot \left(1 - \frac{\varphi}{100}\right)$
	m_{sd}	$Sd_{fact} \cdot A_{acc} \cdot 10$

Table S2: *WEM* state variables and parameters for Cootes Paradise Marsh

Symbol	*Unit*	Value	Variables and Parameters
A	m^2		Areal extent of Cootes Paradise
$A_{(j)}$	m^2		Macrophyte areal coverage in Cootes Paradise
A_{acc}	m^2		Sediment accumulation area
BF_{HH}	$m^3 \cdot day^{-1}$		Backflow from Hamilton Harbour to Cootes Paradise
$Chl\alpha$	$\mu g \cdot L^{-1}$		Chlα concentration in the water column
cDP_{sd}	$\mu g \cdot L^{-1}$		Dissolved phosphorous (DP) concentration in the sediment
cDP_w	$\mu g \cdot L^{-1}$		DP concentration in the water column
$cMAC_{(j)}$	$g \cdot m^{-2}$		Macrophyte biomass density (dry weight)
$cMAC_{AVE}$	$g \cdot m^{-2}$	50	Average macrophyte biomass density (dry weight)
$cPHYT_{(i)}$	$\mu gC \cdot L^{-1}$		Phytoplankton concentration in the water column
$cPHYT_{Back(i)}$	$\mu gC \cdot L^{-1}$		Phytoplankton concentration from Hamilton Harbour
$cPP_{(k)}$	$g \cdot kg^{-1}$		Particulate phosphorus (PP) concentration in the sediment
$cPP_{wM(i)}$	$\mu g \cdot L^{-1}$		PP concentration associated with phytoplankton mortality (i.e., detritus concentration)
cPP_w	$\mu g \cdot L^{-1}$		Water-column PP concentration
cTP_{Back}	$\mu g \cdot L^{-1}$		TP concentration from Hamilton Harbour
$cTSS$	$\mu g \cdot L^{-1}$		Concentration of total suspended solids from the tributaries (Spencer, Chedoke, and Borer's Creeks)
$D_{(i)}$	day^{-1}		Phytoplankton mortality rate

$D_{(j)}$	day^{-1}	Macrophyte mortality rate
DP_{Dif}	$kg \cdot day^{-1}$	Sediment DP diffusive reflux to the water column
DP_{Sd}	$kg \cdot day^{-1}$	Rate of change in the amount of sediment DP
$DP_{SdUP(j)}$	$kg \cdot day^{-1}$	Sediment DP uptake by macrophytes
DP_{w}	$kg \cdot day^{-1}$	Rate of change in the amount of water column DP
DP_{wBack}	$kg \cdot day^{-1}$	DP influx driven by backflow from Hamilton Harbour
DP_{wEXT}	$kg \cdot day^{-1}$	External DP influx from Spencer, Chedoke, Borer's Creeks, CSO, WWTP, precipitation and ground water
DP_{wIN}	$kg \cdot day^{-1}$	Total external DP influx to Cootes Paradise (i.e., $DP_{wBack} + DP_{wEXT}$)
$DP_{wM(i)}$	$kg \cdot day^{-1}$	DP flux released from phytoplankton mortality to the water column
DP_{wOUT}	$kg \cdot day^{-1}$	DP flux from Cootes Paradise to Hamilton Harbour
$DP_{wR(j)}$	$kg \cdot day^{-1}$	DP flux from macrophyte respiration to the water column
$DP_{wUP(i)}$	$kg \cdot day^{-1}$	Water-column DP uptake by phytoplankton
$DP_{wUP(j)}$	$kg \cdot day^{-1}$	Water-column DP uptake by macrophytes
FD	-	Daily fractional ratio of the length of sunlight
$f_i(L)$	-	Function of light limitation on phytoplankton
$f_i(N)$	-	Function of nutrient limitation on phytoplankton
$f_i(T)$	-	Function of temperature limitation on phytoplankton
$f_j(L)$	-	Function of light limitation on macrophytes
$f_j(N)$	-	Function of nutrient limitation on macrophytes
$f_j(T)$	-	Function of temperature limitation on macrophytes

f_{shade}	-		Function of light-shading effect driven by the canopy of meadow and emergent macrophytes
$G_{(i)}$	day^{-1}		Phytoplankton growth rates
$G_{(j)}$	day^{-1}		Macrophyte growth rates
H	cm	40	Sediment thickness in Cootes Paradise
I_o	$MJ \cdot m^{-2} day^{-1}$		Solar radiation on the water surface
$I_{opt(i)}$	$MJ \cdot m^{-2} day^{-1}$	10	Optimal solar radiation for phytoplankton growth
$I_{opt(j=EMG)}$	$MJ \cdot m^{-2} day^{-1}$	18	Optimal solar radiation for emergent macrophytes growth
$I_{opt(j=MDW)}$	$MJ \cdot m^{-2} day^{-1}$	18	Optimal solar radiation for meadow macrophytes growth
$I_{opt(j=SUB)}$	$MJ \cdot m^{-2} day^{-1}$	15	Optimal solar radiation for submerged macrophytes growth
$kext$	m^{-1}		Light extinction coefficient
$kext_{Chl\alpha\ (i=A)}$	$m^2 \cdot mg^{-1}$	0.045	Light extinction coefficient by phytoplankton A
$kext_{Chl\alpha\ (i=B)}$	$m^2 \cdot mg^{-1}$	0.075	Light extinction coefficient by phytoplankton B
$kext_{Chl\alpha\ (i=C)}$	$m^2 \cdot mg^{-1}$	0.24	Light extinction coefficient by phytoplankton C
$kext_{SUB}$	$m^3 \cdot g^{-2}$	$1x10^{-4}$	Light extinction coefficient by submerged macrophytes
$kext_{\varepsilon}$	m^{-1}		Background light extinction coefficient
$KP_{(i=A)}$	$\mu g \cdot L^{-1}$	13	P half-saturation constant for the growth of phytoplankton A
$KP_{(i=B)}$	$\mu g \cdot L^{-1}$	16	P half-saturation constant for the growth of phytoplankton B
$KP_{(i=C)}$	$\mu g \cdot L^{-1}$	25	P half-saturation constant for the growth of phytoplankton C
KP_{MN}	day^{-1}		Mineralization rate of P in the water column
$KP_{sd(j=EMG)}$	$\mu g \cdot L^{-1}$	50	Sediment P half-saturation constant for the growth of emergent macrophytes

$KP_{sd(j=MDW)}$	$\mu g \cdot L^{-1}$	50	Sediment P half-saturation constant for the growth of meadow macrophytes
$KP_{sd(j=SUB)}$	$\mu g \cdot L^{-1}$	35	Sediment P half-saturation constant for the growth of submerged macrophytes
$KP_{w(j=EMG)}$	$\mu g \cdot L^{-1}$	16	Water-column P half-saturation constant for the growth of emergent macrophytes
$KP_{w(j=MDW)}$	$\mu g \cdot L^{-1}$	21	Water-column P half-saturation constant for the growth of meadow macrophytes
$KP_{w(j=SUB)}$	$\mu g \cdot L^{-1}$	10	Water-column P half-saturation constant for the growth of submerged macrophytes
$MAC_{(j)}$	g		Total macrophyte biomass (in dry weight)
m_{sd}	kg		Sediment mass in Cootes Paradise
$P_{(i)}$	$\mu gP \cdot \mu gC^{-1}$		Amount of internal P sequestered in phytoplankton
$P_{max(i)}$	$\mu gP \cdot \mu gC^{-1}$	0.032	Maximum internal P in phytoplankton
$P_{min(i)}$	$\mu gP \cdot \mu gC^{-1}$	0.012	Minimum internal P in phytoplankton
$P_{Sett(k)}$	$kg \cdot day^{-1}$		Settling P flux by phytoplankton from the water column to the sediments (k= G1, G2 and G3)
$P_{up(i)}$	$\mu gP \cdot \mu gC^{-1} day^{-1}$		P uptake rate of phytoplankton from the water column
$PHYT_{(i)}$	kg		Total phytoplankton biomass
$PHYT_{Back(i)}$	$kg \cdot day^{-1}$		Phytoplankton influx from Hamilton Harbour
$PP_{(k)}$	$kg \cdot day^{-1}$		Rate of change in total amount of PP within the sediment
$PP_{Br(k)}$	$kg \cdot day^{-1}$		Sediment burial rate of P
$PP_{Dcp(k)}$	$kg \cdot day^{-1}$		Sediment PP decomposition rate (i.e., sediment DP influx within the sediment pool)
$PP_{IN(k)}$	$kg \cdot day^{-1}$		PP from the water column to the sediment
PP_{MN}	$kg \cdot day^{-1}$		PP mineralization flux (i.e., mineralized DP influx within the water column)
PP_{OUT}	$kg \cdot day^{-1}$		PP flux from Cootes Paradise to Hamilton Harbour

$PP_{rs(k)}$	$kg \cdot day^{-1}$		Sediment PP resuspension flux to the water column
$PP_{sdM(k)}$	$kg \cdot day^{-1}$		PP flux from macrophyte mortality to the sediments (k= G1, G2 and G3)
PP_{Sett}	$kg \cdot day^{-1}$		Total settling PP flux from the water column to the sediment
$PP_{Sett(k)}$	$kg \cdot day^{-1}$		Settling PP flux from the water column to the specific sediments (k= G1, G2 and G3)
PP_{w}	$kg \cdot day^{-1}$		Rate of change in the amount of water column PP
PP_{wIN}	$kg \cdot day^{-1}$		External PP influx from Spencer, Chedoke, Borer's Creeks, CSO, WWTP, precipitation and ground water
$PP_{wM(i)}$	$kg \cdot day^{-1}$		PP flux driven by phytoplankton mortality to the water column
$PP_{wR(j)}$	$kg \cdot day^{-1}$		PP flux derived from macrophyte metabolic loss (e.g., dead tissues)
$R_{(j)}$	day^{-1}		Macrophyte respiration rates
R_{rs}	$mg \cdot m^{-2} \cdot day^{-1}$		Areal sediment resuspension rate
Sd_{ACE}	%	20	Sediment accumulation extent
Sd_{fact}	$g \cdot cm^{-2}$		Sediment mass per unit area (also known as sediment factor)
SSD	$g \cdot cm^{-3}$	2.45	Sediment solid density
T	°C		Water temperature in Cootes Paradise
$T_{opt(i=A)}$	°C	20	Optimal temperature for the growth of phytoplankton A
$T_{opt(i=B)}$	°C	22	Optimal temperature for the growth of phytoplankton B
$T_{opt(i=C)}$	°C	24	Optimal temperature for the growth of phytoplankton C
$T_{opt(j=EMG)}$	°C	25	Optimal temperature for the growth of emergent macrophytes
$T_{opt(j=MDW)}$	°C	25	Optimal temperature for the growth of meadow macrophytes
$T_{opt(j=SUB)}$	°C	26	Optimal temperature for the growth of submerged macrophytes

T_{Ref}	$°C$	20	Reference temperature
T_{sd}	$°C$		Sediment temperature
TP	$\mu g \cdot L^{-1}$		Total phosphorous (TP) concentration in the water column
TP_{IN}	$kg \cdot day^{-1}$		External TP flux into Cootes Paradise (i.e., $DP_{wIN} + PP_{wIN}$)
t	day		Julian date of the year
V	m^3		Water volume of Cootes Paradise
V_{sd}	m^3		Sediment volume in Cootes Paradise
$v_{(i=A)}$	$m \cdot day^{-1}$	0.05	Settling rate of phytoplankton A
$v_{(i=B)}$	$m \cdot day^{-1}$	0.01	Settling rate of phytoplankton B
$v_{(i=C)}$	$m \cdot day^{-1}$	0.001	Settling rate of phytoplankton C
v_{sett}	$m \cdot day^{-1}$	0.03	Settling rate of PP in the water column
z	m		Water depth in Cootes Paradise
z_{SUB}	m	0.4	Maximum survival depth for submerged macrophytes
α_{Rst}	-		Effect of macrophyte restoration (associated with sediment diffusive reflux)
ε_{DepBr}	day^{-1}		Burial deposition coefficient
ε_{rs}	$mg \cdot m^{-2} \cdot day^{-1}$		Resuspension coefficient
$\varepsilon_{\alpha(j)}$	-	0.31	Macrophyte restoration coefficient
$\theta_{(i=A)}$	$°C^{-2}$	0.005	Temperature-dependent coefficient for phytoplankton A
$\theta_{(i=B)}$	$°C^{-2}$	0.006	Temperature-dependent coefficient for phytoplankton B
$\theta_{(i=C)}$	$°C^{-2}$	0.005	Temperature-dependent coefficient for phytoplankton C

$\theta_{(k=G1)}$	-	1.19	Temperature-dependent coefficient for labile sediment decomposition
$\theta_{(k=G2)}$	-	1.19	Temperature-dependent coefficient for refractory sediment decomposition
$\theta_{(k=G3)}$	-	1.18	Temperature-dependent coefficient for inert sediment decomposition
θ_{Dif}	-	1.08	Temperature-dependent coefficient for sediment P diffusion
$\theta_{M(i)}$	$°C^{-1}$	0.069	Temperature-dependent coefficient for phytoplankton mortality
θ_{MN}	$°C^{-2}$	0.004	Temperature-dependent coefficient for PP mineralization
$\theta_{R(j)}$	-	1.08	Temperature-dependent coefficient for macrophyte respiration
$\theta_{\varepsilon 1}$	-	$5x10^{-4}$	Temperature-dependent coefficient for macrophyte growth at below optimal temperature
$\theta_{\varepsilon 2}$	-	$4x10^{-3}$	Temperature-dependent coefficient for macrophyte growth at above optimal temperature
$\theta_{D(j)}$	-	1.08	Temperature-dependent coefficient for macrophyte mortality
$\mu_{Chl\alpha/C}$	$g\ Chl\alpha \cdot g\ C^{-1}$	0.02	Chlα to carbon unit converter
$\mu_{P/DW}$	$g\ P \cdot g\ DW^{-1}$	0.0025	Phosphorus to dry-weight biomass unit converter
τ	$N \cdot m^{-2}$		Sediment bed shear stress
τ_c	$N \cdot m^{-2}$	0.03	Critical sediment bed shear stress
φ	%	85	Sediment porosity
Ψ_{HH}	-	0.34	DP to TP ratio from Hamilton Harbour backflow
$\Psi_{max(j)}$	-	0.5	Maximum fractional areal coverage of macrophytes in Cootes Paradise
$\Psi_{MET(j=EMG)}$	-	0.025	Fraction of P used by emergent macrophyte metabolic activity
$\Psi_{MET(j=MDW)}$	-	0	Fraction of P used by meadow macrophyte metabolic activity
$\Psi_{MET(j=SUB)}$	-	0.5	Fraction of P used by submerged macrophyte metabolic activity

$\Psi_{mP(i)}$	-	0.6	Fraction of P from phytoplankton mortality
$\Psi_{Nut(j=EMG)}$	-	1.65	Weight coefficient of sediment DP preference of emergent macrophytes over water-column DP
$\Psi_{Nut(j=MDW)}$	-	1.2	Weight coefficient of sediment DP preference of meadow macrophytes over water-column DP
$\Psi_{Nut(j=SUB)}$	-	1	Weight coefficient of sediment DP preference of submerged macrophytes over water-column DP
$\Psi_{PP(i,\ k=G1)}$	-	0.6	P transfer fraction from phytoplankton mortality to the sediment G1 (labile)
$\Psi_{PP(i,\ k=G2)}$	-	0.4	P transfer fraction from phytoplankton mortality to the sediment G2 (refractory)
$\Psi_{PP(i,\ k=G3)}$	-	0	P transfer fraction from phytoplankton mortality to the sediment G3 (inert)
$\Psi_{PP(j=EMG,\ k=G1)}$	-	0.2	P transfer fraction from emergent macrophyte mortality to the sediment G1
$\Psi_{PP(j=MDW,\ k=G1)}$	-	0.2	P transfer fraction from meadow macrophyte mortality to the sediment G1
$\Psi_{PP(j=SUB,\ k=G1)}$	-	0.6	P transfer fraction from submerged macrophyte mortality to the sediment G1
$\Psi_{PP(j=EMG,\ k=G2)}$	-	0.8	P transfer fraction from emergent macrophyte mortality to the sediment G2
$\Psi_{PP(j=MDW,\ k=G2)}$	-	0.8	P transfer fraction from meadow macrophyte mortality to the sediment G2
$\Psi_{PP(j=SUB,\ k=G2)}$	-	0.4	P transfer fraction from submerged macrophyte mortality to the sediment G2
$\Psi_{PP(j=EMG,\ k=G3)}$	-	0	P transfer fraction from emergent macrophyte mortality to the sediment G3
$\Psi_{PP(j=MDW,\ k=G3)}$	-	0	P transfer fraction from meadow macrophyte mortality to the sediment G3
$\Psi_{PP(j=SUB,\ k=G3)}$	-	0.4	P transfer fraction from submerged macrophyte mortality to the sediment G3
$\Psi_{PP(k=G1)}$	-	0.1	P transfer fraction from the water-column PP to the sediment G1
$\Psi_{PP(k=G2)}$	-	0.5	P transfer fraction from the water-column PP to the sediment G2
$\Psi_{PP(k=G3)}$	-	0.4	P transfer fraction from the water-column PP to the sediment G3
$\Psi_{Pup(j)}$	-		Macrophyte P uptake ratio between sediment and water column

$\Psi_{R(j)}$	-	0.15	P fraction between dissolved and particulate forms in macrophyte metabolic loss
$\Psi_{rs(k=G1)}$	-	0.4	Resuspension fraction from labile sediment
$\Psi_{rs(k=G2)}$	-	0.4	Resuspension fraction from refractory sediment
$\Psi_{rs(k=G3)}$	-	0.2	Resuspension fraction from inert sediment
Ψ_{Sa}	-	0.81	Maximum fraction of light attenuation driven by macrophyte shading effect
Ψ_{RET}	-	0.5	P retention factor associated with macrophyte tubers and slow decomposed materials
$\omega_{D(j=EMG)}$	day^{-1}	0.0035	Mortality rate of emergent macrophytes at reference temperature
$\omega_{D(j=MDW)}$	day^{-1}	0.005	Mortality rate of meadow macrophytes at reference temperature
$\omega_{D(j=SUB)}$	day^{-1}	0.048	Mortality rate of submerged macrophytes at reference temperature
$\omega_{Dcp(k=G1)}$	day^{-1}	$2x10^{-4}$	Labile sediment decomposition rate
$\omega_{Dcp(k=G2)}$	day^{-1}	$1x10^{-4}$	Refractory sediment decomposition rate
$\omega_{Dcp(k=G3)}$	day^{-1}	$1x10^{-5}$	Inert sediment decomposition rate
ω_{Dif}	day^{-1}	$6.5x10^{-3}$	Sediment diffusion rate to the water column
$\omega G_{(i=A)}$	day^{-1}	2.4	Maximum growth rate of phytoplankton A
$\omega G_{(i=B)}$	day^{-1}	1.9	Maximum growth rate of phytoplankton B
$\omega G_{(i=C)}$	day^{-1}	1.6	Maximum growth rate of phytoplankton C
$\omega G_{(j)}$	day^{-1}	0.06	Maximum gross photosynthetic rate of macrophytes
ω_{HHout}	$m^3 \cdot day^{-1}$		Outflow to Hamilton Harbour
$\omega_{M(i=A)}$	day^{-1}	0.03	Mortality rate of phytoplankton A

$\omega_{M(i=B)}$	day^{-1}	0.01	Mortality rate of phytoplankton B
$\omega_{M(i=C)}$	day^{-1}	0.005	Mortality rate of phytoplankton C
$\omega_{maxUP(i=A)}$	$\mu gP \cdot \mu gC^{-1} day^{-1}$	0.028	Maximum internal P uptake rate of phytoplankton A
$\omega_{maxUP(i=B)}$	$\mu gP \cdot \mu gC^{-1} day^{-1}$	0.023	Maximum internal P uptake rate of phytoplankton B
$\omega_{maxUP(i=C)}$	$\mu gP \cdot \mu gC^{-1} day^{-1}$	0.02	Maximum internal P uptake rate of phytoplankton C
ω_{MN}	day^{-1}	0.006	Mineralization rate at reference temperature
$\omega R_{(j=EMG)}$	day^{-1}	0.019	Respiration rate of emergent macrophytes at reference temperature
$\omega R_{(j=MDW)}$	day^{-1}	0.019	Respiration rate of meadow macrophytes at reference temperature
$\omega R_{(j=SUB)}$	day^{-1}	0.015	Respiration rate of submerged macrophytes at reference temperature
ω_{rs}	day^{-1}	3.5×10^{-5}	Sediment resuspension rate